J. Fluid Mech. (1992), *vol.* 239, *pp.* 157–194
Printed in Great Britain

Spectral large-eddy simulation of isotropic and stably stratified turbulence

By OLIVIER MÉTAIS AND MARCEL LESIEUR

Institut de Mécanique de Grenoble, Institut National Polytechnique de Grenoble, et Université Joseph Fourier, Grenoble, BP 53 X, 38041 Grenoble-Cedex, France

(Received 5 June 1990 and in revised form 21 November 1991)

We first recall the concepts of spectral eddy viscosity and diffusivity, derived from the two-point closures of turbulence, in the framework of large-eddy simulations in Fourier space. The case of a spectrum which does not decrease as $k^{-\frac{5}{3}}$ at the cutoff is studied. Then, a spectral large-eddy simulation of decaying isotropic turbulence convecting a passive temperature is performed, at a resolution of 128^3 collocation points. It is shown that the temperature spectrum tends to follow in the energetic scales a k^{-1} range, followed by a $k^{-\frac{5}{3}}$ inertial–convective range at higher wavenumbers. This is in agreement with previous independent calculations (Lesieur & Rogallo 1989). When self-similar spectra have developed, the temperature variance and kinetic energy decay respectively like $t^{-1.37}$ and $t^{-1.85}$, with identical initial spectra peaking at $k_i = 20$ and $\propto k^8$ for $k \to 0$. In the k^{-1} range, the temperature spectrum is found to collapse according to the law $E_T(k,t) = 0.1\eta\,(\langle u^2\rangle/\epsilon)\,k^{-1}$, where ϵ and η are the kinetic energy and temperature variance dissipation rates. The spectral eddy viscosity and diffusivity are recalculated explicitly from the large-eddy simulation: the anomalous $\propto \ln k$ behaviour of the eddy diffusivity in the eddy-viscosity plateau is shown to be associated with the large-scale intermittency of the passive temperature: the p.d.f. of the velocity component u is Gaussian ($\sim \exp -X^2$), while the scalar T, the velocity derivatives $\partial u/\partial x$ and $\partial u/\partial z$, and the temperature derivative $\partial T/\partial z$ are all close to exponential $\exp -|X|$ at high $|X|$. The pressure distribution is exponential at low pressure and Gaussian at high.

For stably stratified Boussinesq turbulence, the coupling between the temperature and the velocity fields leads to the disappearance of the 'anomalous' temperature behaviour (k^{-1} range, logarithmic eddy diffusivity and exponential probability density function for T). These are the highest-resolution calculations ever performed for this problem. We also split the eddy viscous coefficients into a vortex and a wave component. In both cases (unstratified and stratified), comparisons with direct numerical simulations are performed.

Finally we propose a generalization of the spectral eddy viscosity to highly intermittent situations in physical space: in this *structure-function model*, the spectral eddy viscosity is based upon a kinetic energy spectrum local in space. The latter is calculated with the aid of a local second-order velocity structure function. This structure function model is compared with other models, including Smagorinsky's, for isotropic decaying turbulence, and with high-resolution direct simulations. It is shown that low-pressure regions mark coherent structures of high vorticity. The pressure spectra are shown to follow Batchelor's quasi-normal law: $\alpha C_k^2 \epsilon^{\frac{4}{3}} k^{-\frac{7}{3}}$ (C_k is Kolmogorov's constant), with $\alpha \approx 1.32$.

1. Introduction

It is well known that direct numerical simulations of the Navier–Stokes equations in turbulent situations, which take complete account of all the scales of motion, are limited to relatively small values of the Reynolds number: for instance, direct numerical simulations using pseudo-spectral techniques with 128^3 collocation points allow one to reach a maximum value of $R_\lambda \approx 80$, where R_λ is the Reynolds number based on the Taylor microscale. Hence, high-Reynolds-number turbulence cannot be computed accurately at all scales. In many cases, attention is directed towards the large scales, since they contain most of the energy of the flow. Thus, the small scales have to be modelled through a proper subgrid-scale parameterization.

The problem is extremely difficult and not yet resolved, particularly when working in physical space with finite-difference methods: the large scales are defined with the aid of an adequate spatial filtering of the equations of motion, and the subgrid-scale terms are generally expressed in terms of eddy-coefficients (see, e.g. Rogallo & Moin 1984, for a review). Another approach consists in working in Fourier space, which is possible only if the boundary conditions are simple enough (periodic or free slip for instance). In this case, the large scales correspond to low wavenumbers, and the explicitly resolved scales can be defined by retaining the Fourier wave vectors $\boldsymbol{k}$ such that $k = |\boldsymbol{k}| \leqslant k_c$, where k_c is the cutoff wavenumber: this corresponds to a sharp filter in Fourier space. The time-evolution of the modes within the interior of the sphere of radius k_c is coupled with that of the truncated modes lying outside the sphere. If the latter are simply ignored, and if the viscosity is sufficiently low, it is well known that the system evolves towards an equipartition of energy between the modes (which yields a k^2 kinetic energy spectrum in the case of three-dimensional isotropic turbulence; see Lee 1952). This point can be checked easily with the aid of a direct numerical simulation. Such an equipartition is of course unacceptable if k_c lies in the Kolmogorov $k^{-\frac{5}{3}}$ range. Hence, a subgrid-scale parameterization is needed.

In this paper, we use the concepts of spectral eddy viscosity and eddy diffusivity for this purpose: §2 will recall the essence of the parameterization, and discuss its limitations, especially in the neighbourhood of k_c. Section 3 will present isotropic decay calculations for the velocity and the scalar fields with a direct evaluation of the spectral eddy coefficients and of the probability density functions (p.d.f.) of the various unknowns and of their derivatives. In §4, the influence of a stable stratification will be studied at the same high resolution (128^3). Finally, a new subgrid model taking into account the spatial internal intermittency of turbulence will be presented in §5. This *structure-function model* will, for isotropic turbulence, be compared with the standard spectral eddy viscosity and Smagorinsky's model. Particular emphasis is put on the pressure fluctuations, from statistical, spectral and topological points of view.

2. Eddy viscosity and diffusivity in Fourier space

2.1. *The spectral eddy viscosity in three-dimensional isotropic turbulence*

The concept of k-dependent eddy viscosity was introduced by Kraichnan (1976) for three-dimensional isotropic turbulence, in the following way: if $T_{>k_c}(k,t)$ is the kinetic energy transfer across the cutoff k_c, corresponding to triadic interactions such that $k < k_c$, p and (or) $q > k_c$ (see Lesieur 1987 for details), one can pose

$$\nu_t(k|k_c) = -\frac{T_{>k_c}(k,t)}{2k^2E(k,t)}, \tag{2.1}$$

in such a way that the kinetic energy spectrum $E(k,t)$ in the resolved scales ($k \leqslant k_c$) satisfies

$$\left[\frac{\partial}{\partial t} + 2(\nu + \nu_t(k|k_c))\,k^2\right]E(k,t) = T_{<k_c}(k,t), \tag{2.2}$$

where $T_{<k_c}(k,t)$ is the kinetic energy transfer corresponding to resolved triads such that $k, p, q \leqslant k_c$. Equation (2.2) is exact, but a closure assumption is needed in order to determine $\nu_t(k|k_c)$: Kraichnan (1976) used the test-field model and showed that, in an infinite $k^{-\frac{5}{3}}$ range, the normalized eddy viscosity $\nu_t(k|k_c)/\epsilon^{\frac{1}{3}}k_c^{-\frac{4}{3}}$ is constant up to $k < 0.3k_c$, and displays a sharp positive cusp in the neighbourhood of k_c. Chollet & Lesieur (1981) (see also Chollet 1984, 1985) used the eddy-damped quasi-normal Markovian theory (EDQNM, see e.g. Lesieur 1987 for details) for decaying turbulence with k_c lying in a Kolmogorov inertial range of finite amplitude (about four decades), and found approximately the same results. In the latter analysis, the EDQNM velocity triple-correlations adjustable constant a_1, which is defined precisely in (2.8), was chosen equal to 0.36 in order to recover a value of 1.4 for the Kolmogorov constant (see (2.9)).

Chollet & Lesieur (1981) proposed using the eddy viscosity (2.1) in the Navier–Stokes equations in Fourier space, as a way of modelling the subgrid scales corresponding to $k > k_c$. The equation of motion for the explicit velocity $\hat{\boldsymbol{u}}(\boldsymbol{k},t)$ becomes

$$\left[\frac{\partial}{\partial t} + (\nu + \nu_t(k|k_c))\,k^2\right]\hat{\boldsymbol{u}}(\boldsymbol{k},t) = t_{<k_c}(\boldsymbol{k},t), \tag{2.3}$$

where $t_{<k_c}(k,t)$ stands for the explicit nonlinear triadic interactions, with $\boldsymbol{k}$, $\boldsymbol{p}$ and $\boldsymbol{q}$ such that $k, p, q \leqslant k_c$. As noticed by Lesieur (1987, p. 234), an EDQNM procedure applied to (2.3) yields (2.2), $T_{<k_c}(k,t)$ being written using the general EDQNM expression in terms of kinetic energy spectra, truncated in order to retain only p and $q \leqslant k_c$. It is of course recognized that two-point closures pose problems for describing strong departures from Gaussianity (see Herring 1990). But they seem to predict the right energetics, at least from the point of view of kinetic energy transfer. Hence, the EDQNM eddy viscosity is believed to work nicely from this point of view.

The main criticism of (2.3) concerns the fact that the eddy viscosity $\nu_t(k|k_c)$ does not depend upon the orientation (or 'phase') of the velocity vector $\hat{\boldsymbol{u}}(\boldsymbol{k},t)$ in Fourier space. However, when $k \ll k_c$, and due to the separation of space and time scales, there is no reason, in isotropic turbulence, to expect that the subgrid-scales will instantaneously affect the phase of the velocity field at $\boldsymbol{k}$: this would require a finite time, comparable to the time taken by an error in the small scales to contaminate the large scales in the predictability problem (see e.g. Métais & Lesieur 1986). Hence, an eddy viscosity which correctly extracts the kinetic energy is all right in this case. On the other hand, the validity of this eddy-viscosity concept for large-eddy simulation (LES) purposes is of course questionable in the neighbourhood of k_c, owing to velocity phase shifts between triads of modes k, p, q of the order of k_c. But, since the other existing theories which try to derive analytically the eddy viscosity, such as the renormalization-group techniques (RNG, see e.g. Fournier 1977, or Yakhot & Orszag 1986), or the homogenization techniques (Bègue *et al.* 1987), all assume a separation of scales, there is at present no way of escaping the eddy-viscosity assumption over the whole span of wavenumbers up to k_c.

A modification by Chollet & Lesieur (1981) of Kraichnan's (1976) eddy viscosity, was to employ $[E(k_c)/k_c]^{\frac{1}{2}}$ instead of $\epsilon^{\frac{1}{3}}k_c^{-\frac{4}{3}}$ in order to normalize the eddy viscosity. But they retain for the non-dimensional eddy viscosity the infinite (or large) Kolmogorov-range expression. This yields

$$\nu_t(k|k_c,t) = \nu_t^+(k/k_c)\left[\frac{E(k_c,t)}{k_c}\right]^{\frac{1}{2}}, \tag{2.4}$$

where $\nu_t^+(k/k_c)$ can be approximately expressed as (Chollet 1985):

$$\nu_t^+(k/k_c) = 0.267 + 9.21\,\mathrm{e}^{-3.03(k_c/k)}. \tag{2.5}$$

The advantage of working with (2.4) and (2.5) is that no energy is extracted from the system in the early stage of the cascade, when no energy has yet reached the cutoff. But the modelling is still limited by the fact that (2.5) assumes a wide inertial range about k_c.

For $k \ll k_c$, the spectral eddy viscosity can be considered in a slightly different (and more general) manner: through expansions with respect to the small parameter k/k_c (see e.g. Lesieur 1987, p. 120), the transfer across k_c, calculated using the EDQNM theory, is written

$$\begin{aligned}
T_{>k_c}(k,t) = {} & \frac{2}{15}\left[4E(k)+2k\frac{\partial E}{\partial k}+k^2\frac{\partial^2 E}{\partial k^2}\right]\int_0^{k^2/k_c}\theta_{kkq}\,q^2E(q)\,\mathrm{d}q \\
& -\frac{4}{15}\left[3E(k)+k\frac{\partial E}{\partial k}\right]\frac{E(k)}{k^2}\int_0^{k^2/k_c}\theta_{kkq}\,q^4\,\mathrm{d}q \\
& -\frac{2}{15}\theta_{k,k,k^2/k_c}(k/k_c)^5k^3E(k)^2 \\
& -\frac{2}{15}\theta_{k,k,k^2/k_c}(k/k_c)^3k^3E(k^2/k_c)\left[E(k)-k\frac{\partial E}{\partial k}\right] \\
& -\frac{2}{15}k^2E(k)\int_{k_c}^{\infty}\theta_{kpp}\left[5E(p)+p\frac{\partial E}{\partial p}\right]\mathrm{d}p \\
& +\frac{14}{15}k^4\int_{k_c}^{\infty}\theta_{kpp}\frac{E(p)^2}{p^2}\,\mathrm{d}p.
\end{aligned} \tag{2.6}$$

Here θ_{kpq} is the EDQNM relaxation time for triple correlations, which we will take in this expansion to be in its 'stationary' form:

$$\theta_{kpq} = \frac{1}{\mu(k)+\mu(p)+\mu(q)+\nu(k^2+p^2+q^2)}, \tag{2.7}$$

with

$$\mu(k) = a_1\left(\int_0^k p^2E(p)\,\mathrm{d}p\right)^{\frac{1}{2}}. \tag{2.8}$$

Notice that in the above expansions, θ is not expanded. a_1 is related to the Kolmogorov constant C_k by the following relation (André & Lesieur 1977):

$$a_1 = 0.218C_k^{\frac{3}{2}}. \tag{2.9}$$

It can be shown that, provided that the kinetic energy spectrum decreases above

k_c, with $E(k_c) \leqslant E(k)$, the non-negligible term on the right-hand side of (2.6) is the fifth one, which yields

$$T_{>k_c}(k,t) = -\frac{2}{15}k^2E(k)\int_{k_c}^{\infty}\theta_{0pp}\left[5E(p)+p\frac{\partial E}{\partial p}\right]\mathrm{d}p = -2\nu_t^{\infty}k^2E(k). \tag{2.10}$$

It corresponds to an eddy viscosity given by

$$\nu_t^{\infty} = \frac{1}{15}\int_{k_c}^{\infty}\theta_{0pp}\left[5E(p)+p\frac{\partial E}{\partial p}\right]\mathrm{d}p. \tag{2.11}$$

A similar expression was previously proposed by Kraichnan (1966) using the Lagrangian–history direct interaction closure approximation (LHDIA). Notice that the k^4 *backscatter transfer* (last term on the right-hand side of (2.6)) is here negligible: it becomes important for $k \ll k_1$ (k_1 is the peak of the kinetic energy spectrum), as shown in Lesieur & Schertzer (1978). The resulting infrared $E(k) \propto k^4$ behaviour which occurs when the initial kinetic energy spectrum rises faster than k^4 for low k, has been found in direct numerical simulations starting initially with an energy peak at high wavenumbers (R. S. Rogallo 1988, private communication).

If k_c lies in the middle of an extended $k^{-\frac{5}{3}}$ range, (2.11) allows one to recover $\nu_t(0|k_c,t)$ given by (2.4) and (2.5) (see Chollet 1984), even though k does not belong to this range. This is encouraging for large-eddy simulations of the energy-containing range. But (2.11) is even more general, in the sense that it allows the determination of the eddy viscosity when the spectrum at k_c does not follow the Kolmogorov law. We stress again that this eddy viscosity might describe the subgrid-scale momentum transfers very well, since $k \ll k_c$. If one assumes, for instance, that $E(k) \propto k^{-m}$ above $k_1 \ll k_c$, it is easy to show, using the EDQNM, that, for $m < 3$ (and neglecting molecular viscosity in (2.7))

$$\nu_t^{\infty} = \frac{1}{15a_1}\frac{5-m}{m+1}(3-m)^{\frac{1}{2}}\left[\frac{E(k_c,t)}{k_c}\right]^{\frac{1}{2}}. \tag{2.12}$$

In the particular case $m = \frac{5}{3}$, one recovers the plateau value at $0.441C_K^{-\frac{3}{2}}$, in good agreement with (2.5). However, in the transient stage before a $k^{-\frac{5}{3}}$ spectrum is built up at k_c (with $m > \frac{5}{3}$), the normalized eddy-viscosity plateau will be smaller, since the right-hand side of (2.12) is a decreasing function of m: it is for instance equal to 0.185 instead of 0.267 for $m = 2$. If $m \geqslant 3$, (2.12) is no longer valid. If $m > 3$, θ_{0pp} in (2.11) is approximately constant and of the order of $1/[2a_1[D(k_1)]^{\frac{1}{2}}]$, where

$$D(k_1) = \int_0^{k_1} k^2E(k)\,\mathrm{d}k$$

is the enstrophy contained in the large scales. In this case, the eddy viscosity can be written as

$$\nu_t^{\infty} \approx \frac{5-m}{30a_1}D(k_1)^{-\frac{1}{2}}\int_{k_c}^{\infty}E(k)\,\mathrm{d}k = \frac{1}{30a_1}\frac{5-m}{m-1}D(k_1)^{-\frac{1}{2}}\frac{E(k_c,t)}{k_c}, \tag{2.13}$$

and ν_t^{∞} now scales as $[E(k_c)/k_c]$. In any case, it is still proportional to $(5-m)$, and of same sign. Therefore, it will cancel at $m = 5$, and will become negative for higher values of m. In fact, explicit calculations of the spectral eddy viscosity have been done by Domaradzki *et al.* (1987) with the aid of direct numerical simulations: defining a fictitious cutoff k_c, the kinetic energy transfers between $k < k_c$ and the range p and (or) $q > k_c$ can be evaluated without any closure assumption. The results show very low (and sometimes negative) values for the plateau of $\nu_t(k|k_c)$, normalized

by $[E(k_c,t)/k_c]^{\frac{1}{2}}$. This result, confirmed by similar calculations presented below, is certainly ascribable to the fact that in these calculations, which involve low Reynolds numbers, the kinetic energy spectrum at the cutoff is much steeper than $k^{-\frac{5}{3}}$.

2.2. *The spectral eddy diffusivity*

The above spectral eddy-viscosity concepts have been extended by Chollet (1984, 1985) to the large-eddy simulation of a passive scalar (called here the temperature T, of molecular conductivity κ) in the following way: let $T^T_{>k_c}(k,t)$ be the temperature-variance transfer across the cutoff k_c, and $\kappa_t(k|k_c)$ the spectral eddy-diffusivity, defined by

$$\kappa_t(k|k_c) = -\frac{T^T_{>k_c}(k,t)}{2k^2 E_T(k,t)}, \tag{2.14}$$

$E_T(k,t)$ being the temperature spectrum in the resolved scales. The latter satisfies

$$\left[\frac{\partial}{\partial t} + 2(\kappa + \kappa_t(k|k_c))\,k^2\right] E(k,t) = T^T_{<k_c}(k,t), \tag{2.15}$$

where $T^T_{<k_c}(k,t)$ is the explicit temperature kinetic energy transfer. Again, a closure assumption is needed in order to determine $\kappa_t(k|k_c)$: Chollet (1984, 1985) used the EDQNM in very wide $k^{-\frac{5}{3}}$ Kolmogorov and Corrsin–Oboukhov inertial–convective ranges, with two sets of scalar-velocity triple-correlation constants a_2 and a_3, whose choice is discussed in Herring *et al.* (1982). He found for $\kappa_t(k|k_c)$ expressions analogous to (2.4), that is

$$\kappa_t(k|k_c,t) = \kappa_t^+(k/k_c)\left[\frac{E(k_c,t)}{k_c}\right]^{\frac{1}{2}}, \tag{2.16}$$

where the non-dimensional eddy diffusivity $\kappa_t^+(k/k_c)$ depends upon the choice of the constants: in the first case ('corresponding to LHDIA', $a_2 = 0$), the eddy diffusivity is nearly proportional to the eddy viscosity, with a turbulent Prandtl number $\nu_t(k|k_c)/\kappa_t(k|k_c)$ close to a constant of the order of 0.6. In the second case ('corresponding to DIA', $a_2 = a_3 = a_1$), the normalized eddy diffusivity still displays a plateau up to $k = 0.3k_c$ and a positive cusp above; the turbulent Prandtl number has a plateau value of $\frac{1}{3}$, and a positive cusp where it rises to 0.6.

Again, EDQNM non-local expansions of the temperature subgrid-scale transfer lead, for $k \ll k_c$, to

$$T^T_{>k_c}(k,t) = -2\kappa_t^\infty k^2 E_T(k,t), \tag{2.17}$$

with

$$\kappa_t^\infty = \frac{2}{3}\int_{k_c}^{\infty} \theta^T_{0pp} E(p)\,\mathrm{d}p. \tag{2.18}$$

Here, θ^T_{kpq} is the scalar-velocity triple-correlation relaxation time, expressed here as

$$\theta^T_{kpq} = \frac{1}{\mu'(k)+\mu'(p)+\mu''(q)+\kappa(k^2+p^2)+\nu q^2}, \tag{2.19}$$

with

$$\mu'(k) = a_2\left(\int_0^k p^2 E(p)\,\mathrm{d}p\right)^{\frac{1}{2}}, \tag{2.20}$$

$$\mu''(k) = a_3\left(\int_0^k p^2 E(p)\,\mathrm{d}p\right)^{\frac{1}{2}}. \tag{2.21}$$

An expression similar to (2.18) was previously determined by Kraichnan (1968) (with the aid of LHDIA). One recovers, if k_c lies in an extended Kolmogorov inertial range,

the asymptotic value $\kappa_t(0|k_c,t)$ of (2.16). If one considers a k^{-m} kinetic energy spectrum extending about the cutoff, the corresponding 'plateau' of the turbulent Prandtl number is given, for any m, by

$$Pr_t^{(m)} = (5-m)\frac{a_2+a_3}{20a_1}. \tag{2.22}$$

For $m = \frac{5}{3}$, the corresponding turbulent Prandtl number is

$$Pr_t^{(\frac{5}{3})} = \frac{a_2+a_3}{6a_1}, \tag{2.23}$$

equal respectively to 0.6 and $\frac{1}{3}$ for the two choices of the a_2, a_3 parameters, as stressed above. The corresponding eddy diffusivity is, for $m < 3$,

$$\kappa_t^{\infty} = \frac{4}{3(a_2+a_3)}\frac{(3-m)^{\frac{1}{2}}}{m+1}\left[\frac{E(k_c,t)}{k_c}\right]^{\frac{1}{2}}. \tag{2.24}$$

For $m > 3$, the eddy diffusivity is approximately given by

$$\kappa_t^{\infty} \approx \frac{2}{3(a_2+a_3)}\frac{1}{m-1}D(k_1)^{-\frac{1}{2}}\frac{E(k_c)}{k_c}. \tag{2.25}$$

It is interesting to note that, for $m = 5$, when the eddy viscosity cancels, the eddy diffusivity is finite. This will be confirmed by the direct numerical simulations presented below.

Notwithstanding the difficulties stressed above, we will use in most of the following large-eddy simulations the eddy viscosity defined by (2.4) and (2.5), considering it as an upper bound of the actual eddy viscosity. It will be seen below that this choice does lead to fairly good results for the velocity field in three-dimensional isotropic turbulence. We will also use the eddy diffusivity defined by (2.16), with a turbulent Prandtl number of 0.6, for large-eddy simulations of the passive temperature. Other calculations carried out at a turbulent Prandtl number of 0.3, or even varying with k (see Lesieur & Rogallo 1989), give the same isotropic passive-scalar behaviour. We point out that the above isotropic analysis shows that the eddy coefficients do not depend upon the velocity and temperature fields in the large scales. This is why we believe that the procedure can be applied to anisotropic or inhomogeneous turbulence, provided the subgrid scales $k > k_c$ are isotropic. It has been used successfully to simulate the large scales of stably stratified homogeneous turbulence (Métais & Chollet 1989, see also §4 of the present paper)†, and of the turbulent mixing layer (Comte, Lesieur & Fouillet 1990).

2.3. *The need for high-resolution large-eddy simulations*

In earlier spectral LES studies of homogeneous turbulence (isotropic or stably stratified) carried out by Chollet and colleagues (Chollet & Lesieur 1981; Métais & Chollet 1989), the resolution (32^3) was very low. Encouraging results were obtained concerning the decay laws and the tendency for $k^{-\frac{5}{3}}$ kinetic energy and temperature spectra at the cutoff. But the influence of the cusp in the eddy coefficients could not be seen in the results, and the poor precision in the decay laws did not allow one to distinguish between the unstratified and stratified cases. Higher-resolution calculations (64^3 and 128^3) of three-dimensional isotropic decaying turbulence convecting a passive temperature, done by Lesieur & Rogallo (1989), Lesieur, Métais

† Atmospheric measurements performed by Kaimal *et al.* (1972) give good evidence of small-scale isotropy in stably-stratified turbulence (see also Hunt & Vassilicos 1991 for a review).

& Rogallo (1989) and Métais & Lesieur (1989) showed some 'anomalous behaviour' of the temperature, with respect to EDQNM predictions. The aim of the following sections is to: (*a*) present and discuss the anomalous behaviour of the passive temperature, on the basis of a 128^3 LES calculation with initial spectra peaking at $k_i = 20$. We will in particular examine the probability density functions of the velocity and the temperature; (*b*) perform stratified decay calculations with the same code, in order to investigate whether the above passive-scalar results persist when the temperature is dynamically coupled with the velocity.

3. Decay of three-dimensional isotropic turbulence

The velocity fluctuation $\hat{\boldsymbol{u}}(\boldsymbol{k},t)$ and the passive temperature fluctuation $\hat{T}(\boldsymbol{k},t)$, respective Fourier transforms of $\boldsymbol{u}(\boldsymbol{x},t)$ and $T(\boldsymbol{x},t)$, satisfy the spectral large-eddy simulation equations:

$$(\partial/\partial t + (\nu + \nu_t(k|k_c))\, k^2)\, \hat{\boldsymbol{u}} = \Pi[F[F^{-1}(\hat{\boldsymbol{u}}) \times F^{-1}(\hat{\boldsymbol{\omega}})]], \tag{3.1}$$

$$(\partial/\partial t + (\kappa + \kappa_t(k|k_c))\, k^2)\, \hat{T} = -\mathrm{i}\boldsymbol{k} \cdot F[F^{-1}(\hat{T})\, F^{-1}(\hat{\boldsymbol{u}})], \tag{3.2}$$

$$\boldsymbol{k} \cdot \hat{\boldsymbol{u}}(\boldsymbol{k},t) = 0, \tag{3.3}$$

where F stands for the discrete Fourier transform operator, Π is the projector on the plane perpendicular to $\boldsymbol{k}$, and $\hat{\boldsymbol{\omega}} = \mathrm{i}\boldsymbol{k} \times \hat{\boldsymbol{u}}$ is the vorticity in Fourier space. $\nu_t(k|k_c)$ and $\kappa_t(k|k_c)$ have been defined in §2, and ν and κ are the molecular viscosity and conductivity. In the large-eddy simulation, the molecular coefficients are negligible in comparison to the eddy coefficients: it is in this sense that we will refer to infinite-Reynolds-number large-eddy simulations. For the same reason, no molecular Prandtl number variation need be considered, and we can consider that the calculations correspond to a molecular Prandtl number of the order of 1. In the direct numerical simulations, the eddy coefficients in (3.1) and (3.2) are set equal to zero. The molecular Prandtl number is equal to 1.

The initial kinetic and temperature spectra are identical and equal to

$$E(k,0) = E_T(k,0) = Ak^8 \exp[-4[k/k_i(0)]^2], \tag{3.4}$$

and peak at $k = k_i(0)$. Here, A is chosen such that the initial mean kinetic energy $\frac{1}{2}v_0^2 = \int E(k,0)\,\mathrm{d}k = 1.5$. EDQNM theory predicts that an initial spectrum varying as k^α at low wavenumbers will immediately pick up a k^4 infrared behaviour when $\alpha > 4$ (Lesieur & Schertzer 1978): here, we chose $\alpha = 8$. The ratio between kinetic energy and scalar variance initial spectral peaks is chosen equal to one: we do not investigate here the influence of this parameter (see Antonopoulos-Domis 1981, for a discussion on that point). To solve (3.1)–(3.3), we use pseudo-spectral numerical code (collocation method). Calculations are carried out with 128^3 wavevectors. For time discretization, we use a leap-frog scheme (stabilized by periodic averaging) with a Crank–Nicholson treatment of viscous and conductive terms. Boundary conditions are periodic in the three directions.

3.1. *Large-eddy simulation*

We take $k_i(0) = 20$, and the cutoff wavenumber is $k_c = 60$. The molecular viscosity is taken equal to 10^{-10}. The results of this simulation are described in detail in Lesieur *et al.* (1989). We briefly recall here the main results. In the initial phase, the temperature cascades faster than the velocity field towards small scales, in qualitative agreement with closure results described in Lesieur, Montmory & Chollet (1987). Then, the kinetic energy and the scalar energy respectively decay like $t^{-1.37}$ and $t^{-1.85}$. The agreement with the EDQNM predictions ($t^{-1.38}$ for an initial kinetic

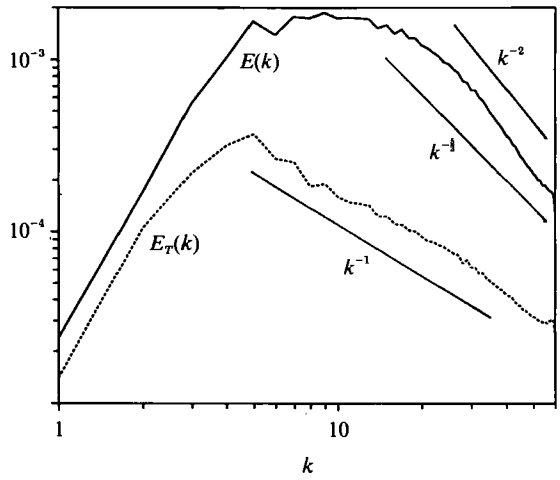

FIGURE 1. Kinetic energy spectrum $E(k)$ and temperature spectrum $E_T(k)$ at $t = 60/v_0 k_1(0)$, large-eddy simulation.

energy spectrum $E(k,0) \propto k^s$ when $k \to 0$, with $s \geqslant 4$) is excellent for the kinetic energy. However, the statistical theory yields a very different law for the decay of the passive-scalar energy ($t^{-1.48}$).

Figure 1 shows, at $t = 60/v_0 k_1(0)$, the kinetic energy and temperature spectra. It is obvious that the temperature variance has decayed much faster than the kinetic energy. The temperature peak, initially equal to k_1, has migrated much faster towards low wavenumbers. This is also in contradiction with the EDQNM predictions of Lesieur *et al.* (1987). The kinetic energy spectrum at the cutoff is close to $k^{-\frac{5}{3}}$, with a Kolmogorov constant, measured from the compensated spectrum $k^{\frac{5}{3}}E(k)$, of the order of 1.5. However, the kinetic energy seems somewhat constrained by k_c, resulting in a slope close to k^{-2} in the vicinity of k_c. The temperature spectrum agrees quite well with Corrsin–Oboukhov's law

$$E_T(k) \sim \eta \epsilon^{-\frac{1}{3}} k^{-\frac{5}{3}}, \tag{3.5}$$

at the cutoff (where η is the temperature dissipation rate), with a constant close 0.9. But the most striking feature of this spectrum is the formation, for $k < 30$, of a range close to a k^{-1} power law. Lesieur & Rogallo (1989) propose that this spectral behaviour is due to a temperature diffusion controlled by the shearing due to velocity gradients at scales $\sim k_1^{-1}$: assuming a temperature variance flux η independent of k, an Oboukhov-type argument yields

$$\eta = k E_T(k,t)/\tau(k_1), \tag{3.6}$$

where $\tau(k_1)$ is the turnover time of k_1. At high Reynolds number, and when turbulence has reached an asymptotic self-similar state, this time may be approximated as $\langle \boldsymbol{u}^2 \rangle / \epsilon$. This yields

$$E_T(k,t) = C_T \eta \frac{\langle \boldsymbol{u}^2 \rangle}{\epsilon} k^{-1}, \tag{3.7}$$

where C_T is a constant. This prediction seems at first sight to be oversimplistic. However, when renormalized by (3.7), the whole time-evolution of the temperature spectrum eventually collapses nicely on a plateau of nearly one decade, with a value of the constant $C_T \approx 0.1$. Details are given in Lesieur *et al.* (1989). Other calculations done with different initial conditions gave the same value for C_T (Lesieur & Rogallo 1989). The phenomenology leading to (3.7) resembles that of the viscous–convective

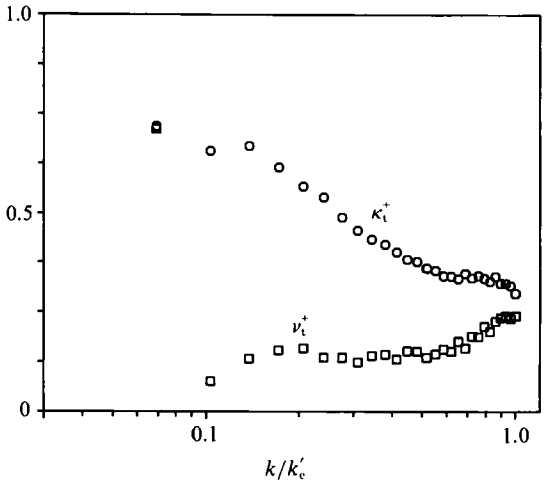

FIGURE 2. Spectral eddy-viscosity ν_t^+ and eddy diffusivity κ_t^+ normalized by $[E(k'_c)/k'_c]^{\frac{1}{3}}$ ($k'_c = 30$), corresponding to figure 1.

range proposed by Batchelor (1959) for high-Prandtl-number turbulence. However, Batchelor's range is located at high k beyond the inertial–convective range, where the turnover time is $(\epsilon/\nu)^{-\frac{1}{2}}$. On the other hand, our present k^{-1} range affects energy-containing eddies, below the inertial–convective range. Actually, this phenomenology is very close to the inertial–convective range in the enstrophy cascade of two-dimensional turbulence, where (3.6) also applies, $\tau(k_1)$ being replaced by $\beta^{-\frac{1}{3}}$ (where β is the enstrophy dissipation rate; see Lesieur 1990). Indeed, some evidence will be given below that large coherent quasi-two-dimensional vortices, randomly oriented, might exist in three-dimensional decaying isotropic turbulence. These vortices might be responsible for the large-scale intermittent character of the passive scalar which will be shown below. As noticed by J. R. Herring (1989, private communication), (3.7) is not invariant under a random-Galilean transformation, due to the presence of $\langle \boldsymbol{u}^2 \rangle$. In fact, this velocity variance arising in (3.7), and used in order to calculate a characteristic straining time at k_1, corresponds to motions $\sim k_1$: it does not comprise any artificial input of energy at $k = 0$ due to a random-Galilean transformation.

We next compute the spectral eddy viscosity and diffusivity, following a method employed by Domaradzki *et al.* (1987) for a direct numerical simulation: one defines a fictitious cutoff wavenumber $k'_c = \frac{1}{2}k_c = 30$, across which the kinetic energy and temperature transfers are evaluated. Since we are dealing with a large-eddy simulation, the latter correspond to triadic interactions such that $k < k'_c$, p and (or) $q > k'_c$ and $p, q < k_c$: they are termed $T_{>k'_c}^{<k_c}(k,t)$ and $T_{k'_c}^{T<k_c}(k,t)$. $T_{>k'_c}^{<k_c}$ satisfies

$$T_{>k'_c}^{<k_c}(k,t) = T_{>k'_c}(k,t) - T_{>k_c}(k,t), \tag{3.8}$$

where $T_{>k'_c}$ and $T_{>k_c}$ are the total kinetic energy transfers across k'_c and k_c (see (2.1)). A similar relation holds for $T_{k'_c}^{T<k_c}$. When divided by $-2k^2E(k,t)$ and $-2k^2E_T(k,t)$, they give the spectral eddy viscosity and diffusivity. Figure 2 shows, at the same time as in figure 1, these functions, normalized by $[E(k'_c)/k'_c]^{\frac{1}{3}}$. The normalized eddy viscosity ν_t^+ displays a plateau of intensity 0.15 far from k'_c. However, for $k \ll k'_c$, (3.8) gives

$$\nu_t^{+\infty<k_c}\left[\frac{E(k'_c)}{k'_c}\right]^{\frac{1}{2}} = \nu_t^{+\infty}\left[\frac{E(k'_c)}{k'_c}\right]^{\frac{1}{2}} - \nu_t^{+\infty}\left[\frac{E(k_c)}{k_c}\right]^{\frac{1}{2}}. \tag{3.9}$$

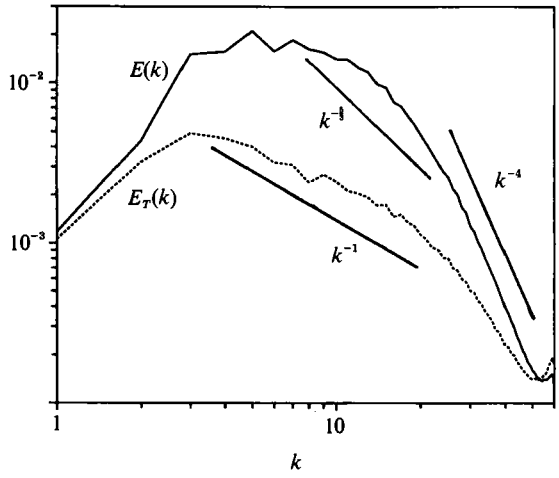

FIGURE 3. Same as figure 1 but for direct simulation and $t = 17/v_0 k_i(0)$.

Assuming that k'_c and k_c lie in a $k^{-\frac{5}{3}}$ range, (3.9) becomes

$$\nu_t^{+\infty} = \frac{\nu_t^{+\infty < k_c}}{1-(k'_c/k_c)^{\frac{4}{3}}}. \tag{3.10}$$

This gives, for the ν_t plateau, a corrected intensity $0.15 \times 1.66 \approx 0.25$, close to the EDQNM value 0.267. The normalized eddy-viscosity cusp is somewhat eroded, due to the proximity of k_i with respect to k_c, in good agreement with Chollet's (1984) EDQNM results. The eddy diffusivity κ_t^+, on the other hand, has no plateau, and decays logarithmically with k in the range where ν_t^+ is constant. In this range, the eddy Prandtl number increases from 0.2 to 0.8. This surprising logarithmic behaviour seems to be related to the existence of the anomalous temperature k^{-1} range, and hence to the large-scale scalar intermittency. A possible way of checking this idea would be to look whether such behaviour exists in two-dimensional isotropic turbulence. To our knowledge, this study has not been carried out yet.

Notice finally that the spectral eddy viscosity given by (2.5) (but with a different set of coefficients) has been used by Batchelor, Canuto & Chasnov (1992) in a large-eddy simulation study of buoyancy-driven turbulence.

3.2. *Direct numerical simulation*

We also performed a direct numerical simulation, with $k_i(0) = 8$, which allows $R_\lambda \leqslant 52$. We let the turbulence evolve until $t = 17/v_0 k_i(0)$. At the end of the run, the kinetic energy decays like $t^{-1.6}$, and the temperature like $t^{-2.6}$. Decay exponents are larger than the EDQNM or the large-eddy simulation ones, because of the small values of the Reynolds and Péclet numbers ($R_\lambda \approx 20$ at the end of the run). Figure 3 shows the kinetic energy and temperature spectra at this time. There is no tendency to any $k^{-\frac{5}{3}}$ ranges, since the Reynolds and Péclet numbers are too low. But the temperature still tends to form a range slightly milder than k^{-1}. However, we have checked that the above scaling (3.7) is no longer valid, certainly because the shearing time at k_i may no longer be expressed as $\langle \boldsymbol{u}^2/\epsilon \rangle$.

Again, we have evaluated directly the spectral eddy-viscosity and diffusivity, from the transfers across k'_c: figure 4 represents the eddy coefficients normalized by

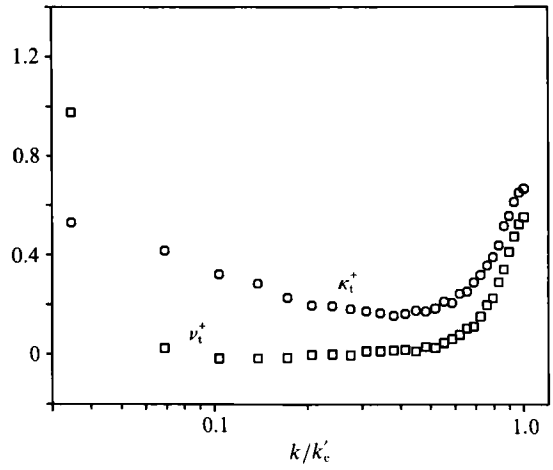

FIGURE 4. Same as figure 2 but for direct simulation and $t = 17/v_0 k_1(0)$.

	u	$\partial u/\partial x$	$\partial u/\partial z$	w	$\partial w/\partial x$	$\partial w/\partial z$	T	$\partial T/\partial x$	$\partial T/\partial z$	t	N
S	−0.012	−0.463	−0.021	0.021	−0.022	−0.435	0.00027	0.0061	0.018	17	0
F	3.01	3.94	4.59	2.98	4.69	3.85	4.02	5.58	5.47	17	0
S	−0.019	−0.490	−0.014	0.023	−0.0039	−0.376	−0.012	0.019	1.027	17	$\frac{1}{3}\pi$
F	3.03	3.99	4.64	3.03	4.84	3.77	3.18	6.02	6.47	17	$\frac{1}{3}\pi$
S	0.077	−0.577	−0.039	0.096	0.047	−0.057	−0.060	0.051	0.599	99	$\frac{1}{3}\pi$
F	3.05	4.31	4.08	3.28	5.59	3.61	3.11	4.75	4.16	99	$\frac{1}{3}\pi$

TABLE 1

$[E(k_c')/k_c']^{\frac{1}{2}}$. Both coefficients exhibit a rapid growth near the cutoff. The plateau of the eddy viscosity is very close to zero, with negative values in the smallest wavenumbers as already noticed by Domaradzki *et al.* (1987). On the other hand the eddy diffusivity exhibits finite values, and behaves logarithmically as in the large-eddy simulation.

In fact, since the slope of $E(k)$ on figure 3 is intermediate between k^{-4} and k^{-5}, it might be that the right scaling should be given by (2.13) and (2.25), still corresponding to a very low eddy viscosity, and a finite eddy diffusivity.

We next examine the probability density function $\mathscr{P}(X)$ for both velocity and scalar fields and their derivatives at the end of the run. Corresponding skewness and flatness factors are given in table 1. The skewness (S) and flatness factors (F) of a distribution f are given by: $S_f = \langle f^3\rangle/\langle f^2\rangle^{\frac{3}{2}}, F_f = \langle f^4\rangle/\langle f^2\rangle^2$; x, y, z are the components of $\boldsymbol{x}$ in a right-handed Cartesian coordinate system, u, v, w are the corresponding components of $\boldsymbol{u}$. As in grid turbulence experiments (Batchelor 1953), figure 5(*a*) shows that $\mathscr{P}(X), X = u$, is close to Gaussian ($S_u \approx 0; F_u \approx 3$). For isotropic turbulence, longitudinal derivative skewness $S_{\partial u/\partial x}$ is a non-dimensional measure of enstrophy production by the nonlinear terms of the equations (enstrophy produced by vortex stretching; see e.g. Orszag 1977): the $\partial u/\partial x$ distribution is then skewed (figure 5*b*). Values for $S_{\partial u/\partial x}$ and $F_{\partial u/\partial x}$ (see table 1) are in good agreement with those obtained, at comparable Reynolds number, in laboratory experiments (Tavoularis, Bennett & Corrsin 1978) and in previous numerical simulations (Orszag & Patterson 1972). $\mathscr{P}(\partial u/\partial z)$ seems close to an exponential function in the wings (figure 5*c*). $F_{\partial u/\partial z}$ differs appreciably from its Gaussian value $F_{\partial u/\partial z} = 4.59$. However,

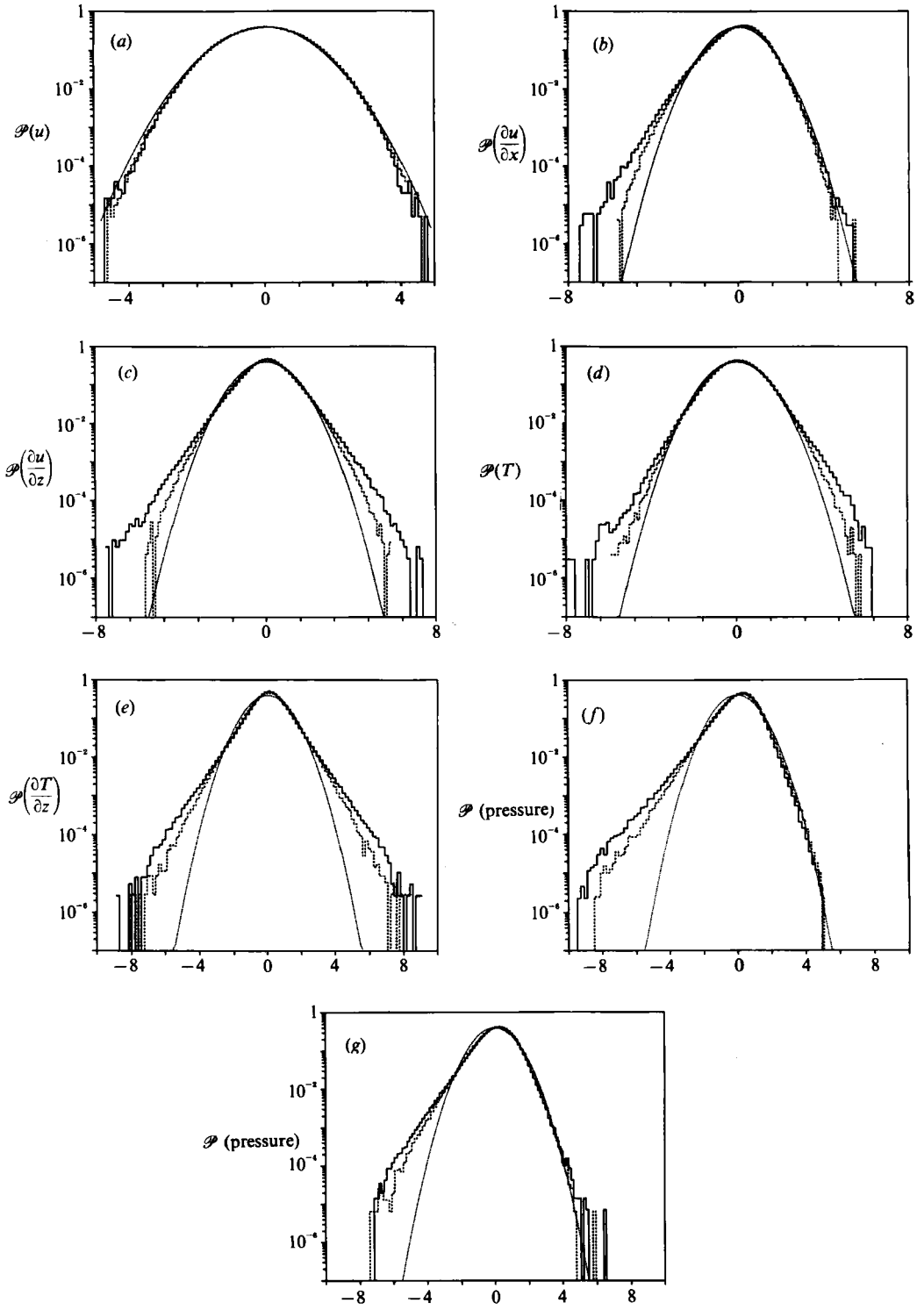

FIGURE 5. Probability density function $\mathscr{P}(X)$: (*a*) $X = u$; (*b*) $X = \partial u/\partial x$; (*c*) $X = \partial u/\partial z$; (*d*) $X = T$; (*e*) $X = \partial T/\partial z$. ----, Large eddy-simulation; ——, direct simulation (the functions are normalized so that their variance is equal to 1); ....., Gaussian distribution. (*f*) X = pressure field: ——, direct simulation; – – – –, Gaussian kinematic field. (*g*) Same as (*f*) for large-eddy simulation.

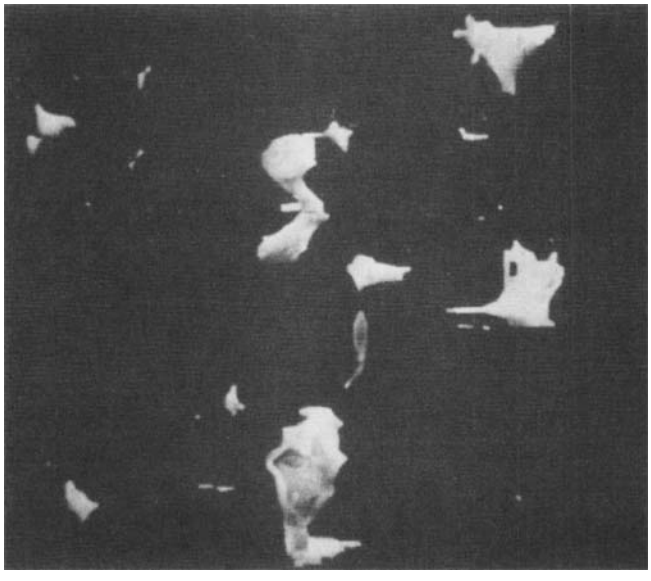

FIGURE 6. Three-dimensional plot of the passive-scalar fluctuation, direct numerical simulation at $t = 17/v_0 k_i(0)$; $\frac{1}{8}$th of the computational domain is represented. It is centred on the instantaneous fluctuations extremum. The grey surface corresponds to 40% of this extremum.

isotropy implies $S_{\partial u/\partial z} \approx 0$. Similar results were found in the lower-resolution isotropic direct numerical simulations performed by Métais & Herring (1989). The reader will find in this reference a discussion of possible analogies with similar findings in various experiments in thermal convection or in turbulent shear flows. High-Reynolds-number experimental measurements show that the tails of the velocity-derivative probability density function deviate from truly exponential behaviour (Gagne 1987; Castaing, Gagne & Hopfinger 1990). Several theoretical models have been proposed to explain this deviation (Kraichnan 1990; Castaing *et al.* 1990). Notice that in our calculations as well as in others done by Yamamoto & Hosokawa (1988) and Vincent & Meneguzzi (1991), the p.d.f. of the various vorticity components is also highly non-Gaussian in the wings, as in two-dimensional turbulence calculations done by McWilliams (1989). In the latter case, this distribution is due to the condensation of vorticity into spots, that is a vorticity large-scale intermittency: the pressure lows, which are well correlated with intense vorticity, should then be non-Gaussian, in such a way that the pressure p.d.f. is expected to be highly skewed towards low values.

Figures 5(*d*) and 5(*e*) show respectively the probability density of T and $\partial T/\partial z$: surprisingly, not only $\partial T/\partial z$, but also T, is close to an exponential function. Owing to the isotropy of the velocity field, neither the temperature fluctuations nor their derivatives are skewed (see table 1). The scalar-variance flatness is 4, which is different to the Gaussian value found in the experiment of Sreenivasan *et al.* (1980) and the simulation of Kerr (1985). The forcing introduced in Kerr's simulation in order to maintain steady-state turbulence could be the origin of the difference. The departure from Gaussianity for the scalar-fluctuation p.d.f. indicates a large-scale intermittency. Indeed, the temperature presents very strong fluctuations in small spatial regions, with quiescent regions being more likely the result of random sampling. This is illustrated on figure 6, which represents a three-dimensional isosurface (40% of the extremum) of the scalar fluctuations. This plate shows, at the

end of the run, $\frac{1}{8}$th of the computational domain centred on the extremum. Extremely concentrated scalar structures are apparent. The departure from Gaussianity is stronger for the temperature derivative than for the velocity derivative. Larger values for the scalar derivative flatness, compared to the velocity derivative flatness, are in good agreement with experimental values (Antonia *et al.* 1978; Sreenivasan *et al.* 1980; Antonia *et al.* 1982). The weaker velocity intermittency could be attributable to the non-local effect of the pressure which tends to redistribute the velocity fluctuations.

Figure 5(*a–e*) also shows the p.d.f.s of u, $\partial u/\partial x$, $\partial u/\partial z$, T, $\partial T/\partial z$ as given by the large-eddy simulation of §3.1, at the end of the run. The higher p.d.f. in the wings obtained in the direct numerical simulation might be due, as suggested by one referee, to the lower kinetic energy peak $k_i(0)$, implying that the small scales are better resolved.

Figures 5(*f*) and 5(*g*) show the pressure p.d.f. respectively for the direct numerical simulation and the large-eddy simulation using the structure function model which will be described in §5: this p.d.f. is compared with that of a fictitious pressure field calculated from a Gaussian velocity field of same kinetic energy spectrum. The highly skewed shape might be evidence of the large-scale vorticity intermittency advocated above in the case of two-dimensional turbulence. However, this is also shared by the kinematic Gaussian evaluation, so that it is difficult to interpret this result in terms of coherent structure dynamics. Notice also that we have not plotted the pressure p.d.f. for the LES using the spectral eddy viscosity, but it is feasible that it will behave in the same manner.

3.3. *Discussion*

The spectral large-eddy and direct numerical simulations of decaying turbulence described here show anomalous behaviour of a convected passive temperature. The kinetic energy decay is in good agreement with statistical theory predictions (Herring *et al.* 1982) and laboratory experiments (Yeh & Van Atta 1973; Warhaft & Lumley 1978). For the passive scalar on the other hand, the ratio L/L_T of the respective velocity and temperature integral lengthscales shifts from 1 initially to 0.76 at the end of our run. This implies a temperature decay weaker than the kinetic energy decay, if one accepts the phenomenological prediction of Corrsin (1964) that

$$\alpha_E/\alpha_T \sim (L_T/L)^{\frac{2}{3}}, \tag{3.11}$$

where α_E and α_T are respectively the kinetic energy and temperature variance decay exponents (see Lesieur 1987 for details and Herring *et al.* 1982 for the role of the Reynolds number). However, α_T is found in the large-eddy simulations to be significantly higher than α_E. Similar findings have been made by Warhaft & Lumley (1978) in their heated-grid experiment in the case of strong heating (see their figure 13), although they have attributed this unexpected behaviour to the relatively high level of anisotropy. For weaker heating, their findings were much closer to theoretical predictions. Moderate-Reynolds-number experiments by Yeh & Van Atta (1973) and by Warhaft & Lumley (1978), where the temperature is injected at the same scale as the kinetic energy, show a temperature spectral range of slope $-\frac{3}{2}$, although no inertial range is apparent for the corresponding kinetic energy spectrum. In high-Reynolds-number EDQNM calculations, with the same type of initial conditions, the temperature spectrum also displays a well-defined $k^{-\frac{3}{2}}$ slope before establishing a $k^{-\frac{5}{3}}$ inertial–convective range and decaying self-similarly (Herring *et al.* 1982; Lesieur *et al.* 1987). Furthermore, the test field model closure calculations of Herring (1990) indicate a fairly good agreement with the LES of Lesieur & Rogallo (1989) except for

a steeper temperature slope given by the closure. The shallower slope given by the LES as compared to the test-field model calculations could be the result of the strong large-scale scalar intermittency which cannot be reproduced by the statistical theory. This suggests that the *anomalous* temperature slopes observed in the experiments and in the closure calculations are the analogue of the k^{-1} temperature slope observed in the present simulations, and could be attributable to the shearing of the scalar by the large-scale velocity gradients. The question to be asked concerns the possible transient nature of this k^{-1} spectrum. However, it behaves self-similarly in our calculation.

Atmospheric and oceanic measurements of small-scale turbulence seem to confirm the universal nature of the velocity spectrum in the Kolmogorov inertial range. However, they suggest that the Corrsin–Oboukhov theory does not provide a universal description of (passive) temperature fluctuations in water nor in air (see e.g. Williams & Paulson 1977; Mestayer 1982; Gargett 1985). Gargett's (1985) proposal that this could be explained by differences in the degree of intermittency in energy dissipation and temperature diffusion seems to be confirmed by the present results. From a theoretical viewpoint, Van Atta (1971) applied Kolmogorov's (1962) lognormal theory to the prediction of corrections of Corrsin–Oboukhov's law, due to intermittency. This theory, applied to large-Reynolds-number oceanic data by Gargett (1985), produces the right qualitative effects of decreasing the spectral slope of the inertial–convective range. In fact, it has been shown experimentally by Anselmet *et al.* (1984) and Antonia *et al.* (1984) that velocity and temperature structure functions of high order depart from the lognormal prediction.

4. Stably stratified turbulence

The scalar, which is still called the temperature (but it may be the potential temperature for an ideal gas) is no longer passive but now coupled with the velocity field. The velocity and temperature fields satisfy the LES-modified Boussinesq set:

$$(\partial/\partial t + (\nu + \nu_t(k|k_c))\, k^2)\, \hat{\boldsymbol{u}} = \Pi[F[F^{-1}(\boldsymbol{u}) \times F^{-1}(\hat{\boldsymbol{\omega}})] + z\hat{T}], \tag{4.1}$$

$$(\partial/\partial t + (\kappa + \kappa_t(k|k_c))\, k^2)\, \hat{T} = -N^2\hat{w} - \mathrm{i}\boldsymbol{k} \cdot F[F^{-1}(\hat{T})\, F^{-1}(\hat{\boldsymbol{u}})], \tag{4.2}$$

$$\boldsymbol{k} \cdot \hat{\boldsymbol{u}}(\boldsymbol{k}, t) = 0. \tag{4.3}$$

z is directed towards the vertical, and w is the vertical velocity. T is proportional to the temperature deviation θ' from the mean temperature profile $\bar{\theta}(z)$; $T = g\theta'/\theta_0$, with θ_0 the volume-averaged value of $\bar{\theta}(z)$ and g the acceleration due to gravity (gravity vector: $\boldsymbol{g} = (0, 0, -g)$). N is the (constant) Brunt–Väisälä frequency:

$$N = \left(\frac{g}{\theta_0}\frac{\mathrm{d}\bar{\theta}}{\mathrm{d}z}\right)^{\frac{1}{2}}. \tag{4.4}$$

We have assumed in (4.1) and (4.2) that the isotropic subgrid-scale modelling of momentum and temperature is still valid in the stratified case, provided that turbulence should be isotropic for $k > k_c$.

In order to economically describe axisymmetric turbulence, Herring (1974) used Craya's (1958) decomposition of the incompressible velocity field (in Fourier space) $\hat{\boldsymbol{u}}(\boldsymbol{k})$ into orthogonal components $\hat{\boldsymbol{u}}_1$ and $\hat{\boldsymbol{u}}_2$:

$$\hat{\boldsymbol{u}}(\boldsymbol{k}, t) = \hat{\boldsymbol{u}}_1(\boldsymbol{k}, t) + \hat{\boldsymbol{u}}_2(\boldsymbol{k}, t), \tag{4.5}$$

with

$$\hat{\boldsymbol{u}}_1(\boldsymbol{k}, t) = \hat{\phi}_1(\boldsymbol{k}, t)\, \boldsymbol{e}_1(\boldsymbol{k}), \tag{4.6}$$

$$\hat{\boldsymbol{u}}_2(\boldsymbol{k}, t) = \hat{\phi}_2(\boldsymbol{k}, t)\, \boldsymbol{e}_2(\boldsymbol{k}), \tag{4.7}$$

where
$$\boldsymbol{e}_1(\boldsymbol{k}) = (\boldsymbol{k}\times\boldsymbol{g})/|(\boldsymbol{k}\times\boldsymbol{g})| \tag{4.8}$$

and
$$\boldsymbol{e}_2(\boldsymbol{k}) = \boldsymbol{k}\times(\boldsymbol{k}\times\boldsymbol{g})/|\boldsymbol{k}\times(\boldsymbol{k}\times\boldsymbol{g})|. \tag{4.9}$$

$\hat{\boldsymbol{u}}_1$ is horizontal and horizontally non-divergent, whereas $\hat{\boldsymbol{u}}_2$ has no vertical vorticity. These properties have led Riley, Metcalfe & Weissman (1981) to use (ϕ_1, ϕ_2) as a method of identifying the turbulent ('vortical') component and the 'internal gravity wave' component of stably stratified turbulent flows. Lilly (1983) developed an equivalent formulation in physical space. However, this identification is a simplication: for unstratified flow, the same decomposition can be performed, ϕ_1 and ϕ_2 are then in equipartition and the above terminology is not relevant (see Métais & Herring 1989; Staquet & Riley 1989 for details). However, we note that $(\hat{\boldsymbol{u}}_1, \hat{\boldsymbol{u}}_2)$ is a convenient representation of the turbulence, which has been extensively used in anisotropic spectral models of turbulence in order to investigate the non-isotropic effects of solid-body rotation and stable stratification (see e.g. Cambon & Jacquin 1989; Cambon 1989). For convenience we call $\boldsymbol{\Phi}_1(\boldsymbol{k})$, the intensity associated with $\hat{\phi}_1$, 'vortex' kinetic energy spectrum:

$$\boldsymbol{\Phi}_1(\boldsymbol{k}) = \tfrac{1}{2}\langle\hat{\phi}_1(-\boldsymbol{k})\,\hat{\phi}_1(\boldsymbol{k})\rangle \tag{4.10}$$

and $\boldsymbol{\Phi}_2(\boldsymbol{k})$ the corresponding 'wave' kinetic energy spectrum.

If slightly displaced, the available potential energy of a particle in a stably stratified medium, is proportional to the square of its (small) vertical displacement ζ from its equilibrium position z. Its temperature deviation from the ambient temperature at height $z+\zeta$ is $\theta' = \zeta \mathrm{d}\bar{\theta}(z)/\mathrm{d}z$. Therefore, the particle's available potential energy is proportional to θ'^2 (see e.g. Lighthill 1978). Since we consider a constant N, one can check that the available potential energy spectrum is

$$P(\boldsymbol{k}) = \frac{1}{2}\frac{\langle\hat{T}(-\boldsymbol{k})\hat{T}(\boldsymbol{k})\rangle}{N^2} \tag{4.11}$$

and that the sum of the kinetic energy and available potential energy is conserved by the nonlinear terms in the equations of motion.

We next consider $T^1_{>k_c}(\boldsymbol{k},t)$ and $T^2_{>k_c}(\boldsymbol{k},t)$, the vortex and wave kinetic energy transfers across a cutoff wavenumber k_c. For anisotropic turbulence, they obviously depend on the orientation of the wave vector $\boldsymbol{k}$. We then define eddy-viscosity coefficients

$$\nu^i_t(\boldsymbol{k}|k_c) = -\frac{T^i_{>k_c}(\boldsymbol{k},t)}{2k^2\boldsymbol{\Phi}_i(\boldsymbol{k},t)}, \quad i = 1,2, \tag{4.12}$$

such that $\boldsymbol{\Phi}_i(\boldsymbol{k},t)$, $i = 1,2$ in the resolved scales ($k \leqslant k_c$) satisfy

$$\left[\frac{\partial}{\partial t} + 2(\nu + \nu^i_t(\boldsymbol{k}|k_c))\,k^2\right]\boldsymbol{\Phi}_i(\boldsymbol{k},t) = T^i_{<k_c}(\boldsymbol{k},t) + \mathscr{B}_i, \tag{4.13}$$

with $T^i_{<k_c}$ the explicit transfers. $\mathscr{B}_1 = 0$ and $\mathscr{B}_2$ involves spectral covariances $\phi_2 - T$. In the following sections, the dependency of the eddy-viscosity and eddy-diffusivity coefficients on the wavevector orientation will be discarded. We will consider coefficients obtained from isotropically accumulated transfers and spectra, and which are functions of the modulus of $\boldsymbol{k}$. We also define

$$\nu^{+i}_t(k/k_c) = \nu^i_t(k|k_c)\left[\frac{E(k_c)}{k_c}\right]^{-\frac{1}{2}}. \tag{4.14}$$

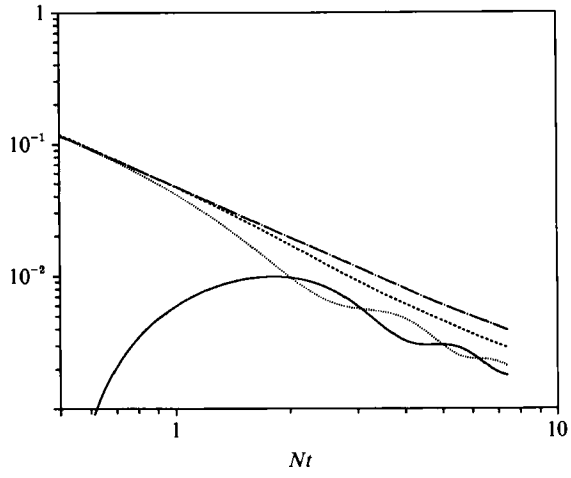

FIGURE 7. Time evolution of the 'vortex' kinetic energy $\bar{\Phi}_1$ (----), 'wave' kinetic energy $\bar{\Phi}_2$ (.....), potential energy $\bar{P}$ (——) and total wave energy $\bar{\Phi}_2+\bar{P}$ (—·—). The time is normalized by $N = 1.047$.

One can see that $\nu_t(k|k_c)$ (see (2.1)) satisfies

$$\nu_t(k)\,E(k) = \nu_t^1(k)\,\Phi_1(k) + \nu_t^2(k)\,\Phi_2(k). \tag{4.15}$$

Starting with the same initial velocity spectrum as in the isotropic case, we let the turbulence evolve until it reaches a fully developed state. Then, at this time t_0, the stratification is turned on. N is chosen such that the initial effects are dominant over the stratification effects (large-Froude-number regime). The initial temperature fluctuations are taken equal to zero and will build up due to the mean stratification. As in the isotropic case, we will consider successively large-eddy and direct numerical simulations.

4.1. *Large-eddy Boussinesq simulation*

We choose $N = 1.047$ $t_0 = 17/v_0 k_i(0) = 0.47N^{-1}$ and let the turbulence decay until $t_f = 257/v_0 k_i(0) = 7.1N^{-1}$. We define the Froude number: $Fr(t) = v/LN$, with $v^2 = 2\int E(k)\,\mathrm{d}k$, and $L = v^3/\epsilon$. The initial Froude number $Fr(t_0) = 3.7$. Figure 7 shows $\bar{\Phi}_1(t)\,(=\int \Phi_1\,\mathrm{d}\boldsymbol{k})$, $\bar{\Phi}_2(t)$, $\bar{P}(t)$ and $\bar{\Phi}_2(t)+\bar{P}(t)$. The time unit is N^{-1}. The results are qualitatively similar to those obtained by Métais & Herring (1989) (64^3 spectral DNS) and by Métais & Chollet (1989) (32^3 spectral LES). The available potential energy grows from zero until it is of the same order as the kinetic energy. Then ϕ_2 takes on the character of gravity waves, thus modulating the decay of potential energy by a periodic exchange with the wave kinetic energy. $\bar{\Phi}_1$ does not show the oscillations characteristic of $\bar{\Phi}_2$ and $\bar{P}$, which indicates that (ϕ_1, ϕ_2) are good discriminators (in this case) between waves and turbulence. The total internal wave energy $(\bar{\Phi}_2+\bar{P})$ also does not exhibit oscillations, showing that it is equally divided between the kinetic and potential forms. Figure 8 shows the time evolution of the instantaneous decay exponents α_V and α_W defined such that $\bar{\Phi}_1(t)$ and $\bar{\Phi}_2(t)+\bar{P}(t)$ are respectively locally tangent to t^{α_V} and t^{α_W} decay laws. The isotropic kinetic energy decay exponent is also plotted. Compared to the unstratified case, the vortex kinetic energy undergoes initially a higher damping due to the available potential energy buildup. Simultaneously, the wave energy follows roughly an isotropic decay. Subsequently, all decay exponents are reduced. However, their decrease in time is modulated by the periodic exchange between wave and vortex energies. We will call

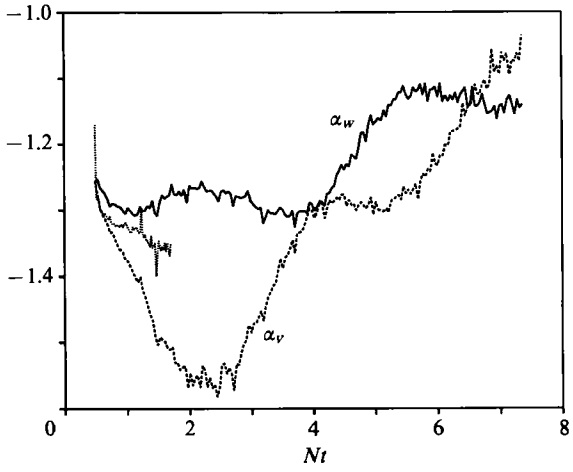

FIGURE 8. Time variations of the instantaneous decay exponents α_v of $\bar{\Phi}_1(t)$ (stratified case: ——; unstratified case: .....) and α_w of $\bar{\Phi}_2(t)+\bar{P}(t)$ (stratified case: ——).

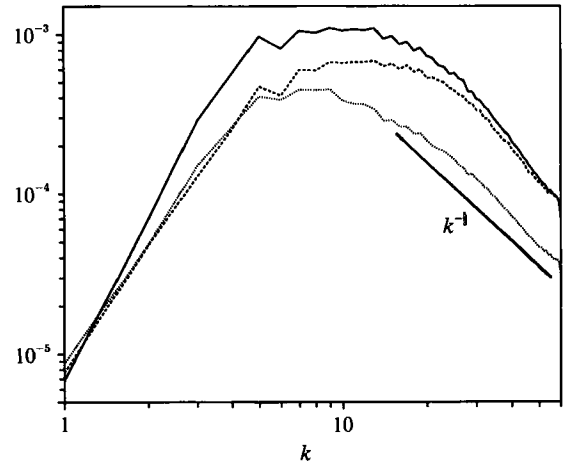

FIGURE 9. 'Vortex' kinetic energy spectrum $\Phi_1(k)$ (——), 'wave' kinetic energy spectrum $\Phi_2(k)$ (– – – –), and potential energy spectrum $P(k)$ (.....) at $t = 1.48N^{-1}$, large-eddy simulation.

the phase where α_V becomes significantly lower than the isotropic decay exponent ($t > 5N^{-1}$) the 'collapsed' state. Before that, the Froude number remains large and the spectrum of the turbulent component (ϕ_1) is weakly affected by the stratification as will be shown below. The average rate of decay for available potential energy is comparable with the vortex energy decay. Therefore, there is a drastic difference in the temperature decay rates between the unstratified and stratified cases. Thus, we focus here on the influence on the temperature field of the velocity–density coupling.

4.1.1. *Pre-collapse phase*

Figure 9 shows the vortex kinetic, wave kinetic and available potential energy spectra at $t = 1.48N^{-1}$ ($Fr = 1.3$). The temperature spectrum has lost the anomalous character it had in the isotropic case, and looks quite similar to the vortex kinetic energy spectrum. The flow is nearly isotropic in the smallest scales: $\Phi_1(k) \approx \Phi_2(k)$ at large k.

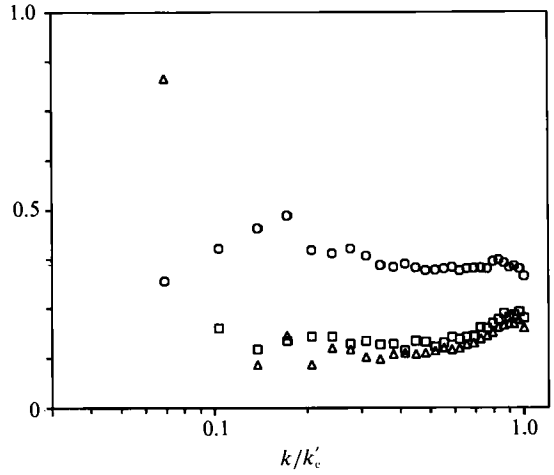

FIGURE 10. Spectral eddy-viscosities ν_t^{+1} (□) and ν_t^{+2}(△) (see (4.14)), and eddy diffusivity κ_t^+ (○) normalized by $[E(k_c')/k_c']^{\frac{1}{2}}$ ($k_c' = 30$), corresponding to figure 8.

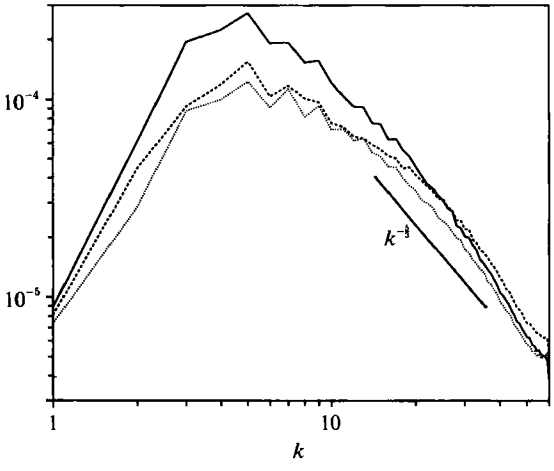

FIGURE 11. Same as figure 9 but at $t = 7.42N^{-1}$.

Figure 10 is the analogue of figure 2 for the stratified case. Both components ν_t^{+1} and ν_t^{+2} are represented. Both coefficients are almost identical and do not differ from the isotropic eddy viscosity previously found. The normalized eddy diffusivity now displays a plateau in the small wavenumbers. The eddy Prandtl number exhibits a near constant value of 0.45. Surprisingly, this behaviour is much closer to the *EDQNM* predictions for passive scalars although, through buoyancy, the temperature is now coupled with the velocity field.

4.1.2. *Post-collapse phase*

At the end of the run, $Fr = 0.18$. Figure 11 is the analogue of figure 9 at $t = 7.42N^{-1}$. The large scales are dominated by the vortex kinetic energy and the small scales by the wave energy. Stratification inhibits the spectral transfer of energy towards small scales, leaving less energy in the latter (Métais & Herring 1989). The eddy coefficients at that time are globally reduced as compared to the pre-collapse phase and exhibit a well-marked growth near the cutoff wavenumber because of the

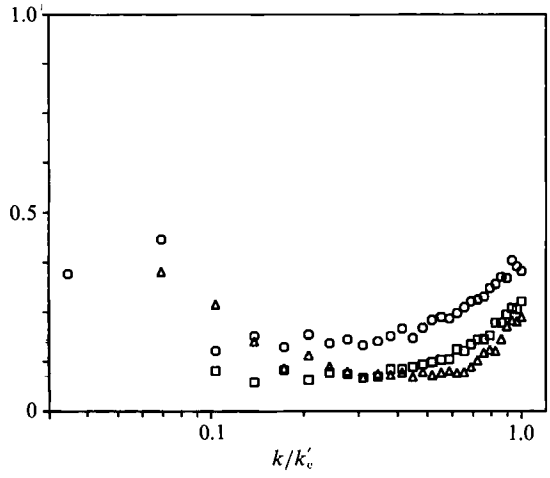

FIGURE 12. Same as figure 10 but at $t = 7.42N^{-1}$.

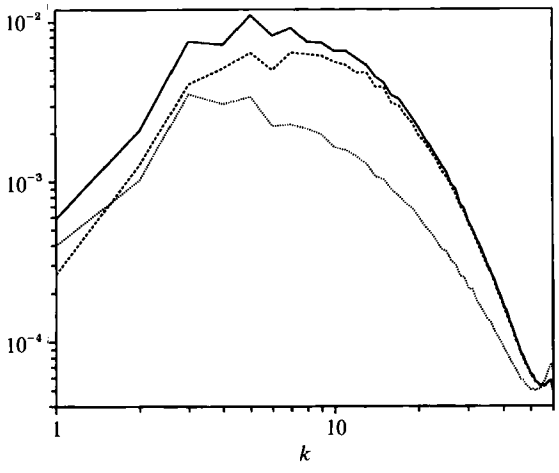

FIGURE 13. Same as figure 9 but for direct simulation and at $t = 1.233N^{-1}$.

shifting of the spectral maxima towards small wavenumbers (figure 12). The plateau intensity for ν_t^{+1} is ≈ 0.09. ν_t^{+2} exhibits the same constant value at intermediate scale but increases with decreasing wavenumber at large scale. The eddy Prandtl number is close to the previous value $Pr \approx 0.475$.

4.2. *Direct Boussinesq simulations*

The initial velocity field is the one obtained in §3.2 ($t_0 = 3.46/v_0 k_i(0)$). The parameters are: $N = 1.047$, $Fr(t_0) = 1.5$. Figures 13 and 14 show respectively the vortex kinetic energy, wave kinetic energy and available potential energy spectra at $t_1 = 17/v_0 k_i(0) = 1.2N^{-1}$ ($Fr(t_1) = 2$) and at the end of the run $t_f = 99/v_0 k_i(0) = 6.8N^{-1}$ ($Fr(t_f) = 0.25$). Comparing with figures 9 and 11, we see that the previously described large-eddy Boussinesq simulation allows for the correct qualitative spectral behaviour of the large scales. The spectral eddy viscosity and diffusivity coefficients are calculated at t_1 and t_f (figures 15 and 16). At a later time, the Kolmogorov wavenumber decrease forces us to choose $k_c' = 15$ instead of 30 in order to escape from the dissipative range. As in the LES, the eddy diffusivity exhibits a

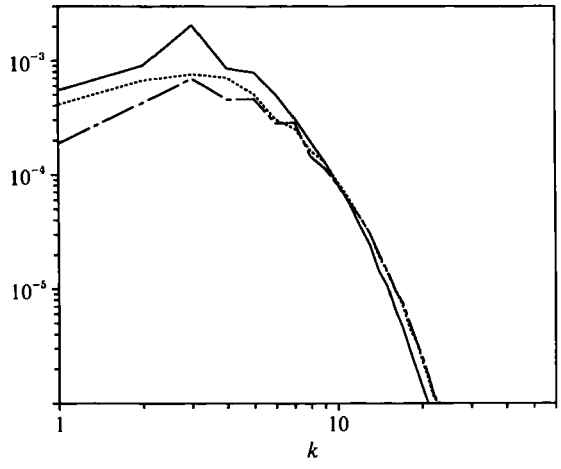

FIGURE 14. Same as figure 13 but at $t = 7.17N^{-1}$.

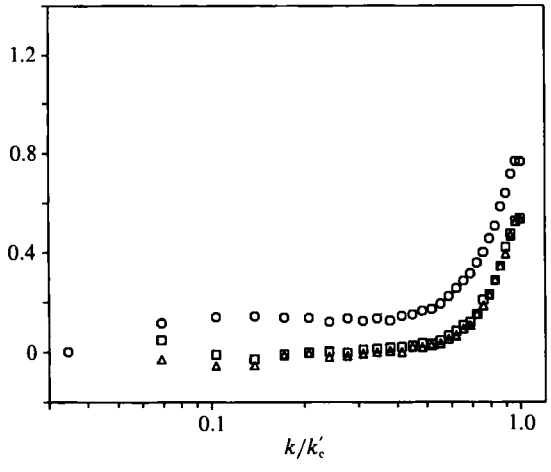

FIGURE 15. Same as figure 10 but for calculation corresponding to figure 13.

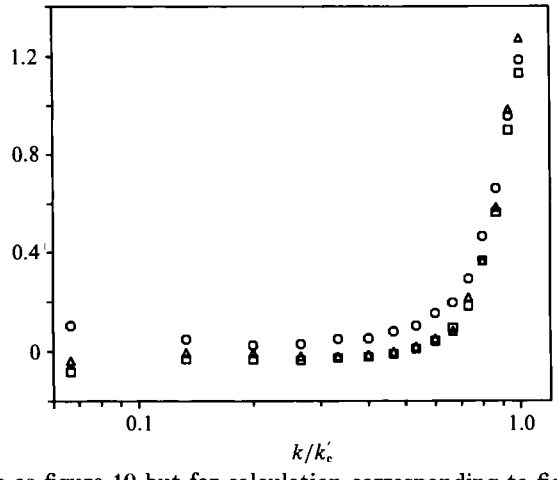

FIGURE 16. Same as figure 10 but for calculation corresponding to figure 14 and $k_c' = 15$.

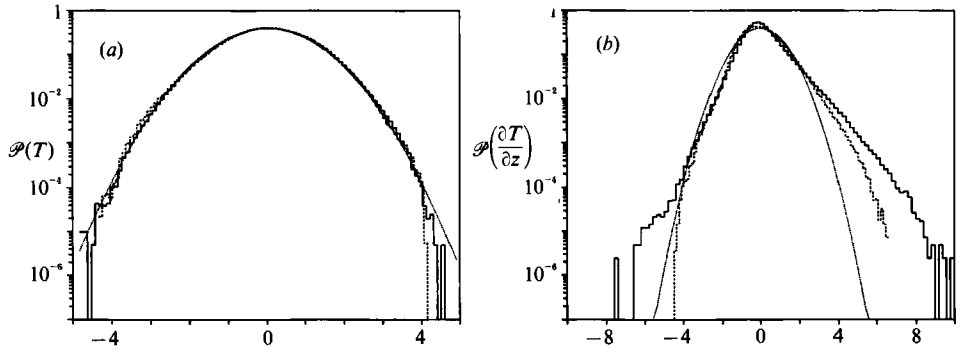

FIGURE 17. Probability density function $\mathscr{P}(X)$: (*a*) $X = T$; (*b*) $X = \partial T/\partial z$. Stably stratified direct simulation: $t = 1.233N^{-1}$ (——); $t = 7.17N^{-1}$(– – – –); together with a Gaussian distribution (.....).

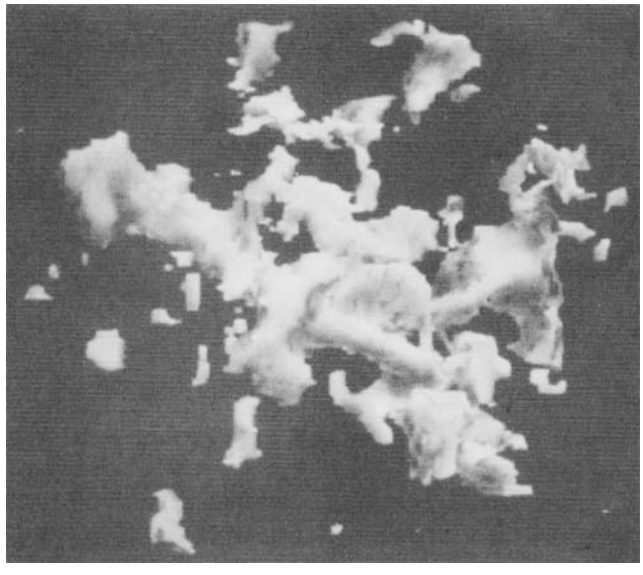

FIGURE 18. Same as figure 6 but for stably stratified direct simulation. The z-axis is the perspective axis.

constant value at large scales during both pre- and post-collapse phases. Its intensity is reduced after the collapse. ν_t^{+2} slightly increases at large scales.

As opposed to the isotropic case, both velocity and temperature probability densities ($\mathscr{P}(X), X = u$ and $X = T$) exhibit a Gaussian behaviour (see figure 17*a* and table 1). This indicates the disappearance of large-scale temperature intermittency. Figure 18, which is analogous to the stratified case of figure 6, illustrates this point. However, small-scale temperature intermittency remains. The probability density for $X = \partial T/\partial z$ exhibits a very asymmetrical shape before and after the collapse (figure 17*b*). The corresponding skewness factors have large positive values (table 1). One can propose the following explanation. Since we start with zero temperature fluctuations, the dominant term of the right-hand side of (4.2) is initially the buoyancy term. Neglecting the diffusive effects, the equation of evolution of $T(\boldsymbol{x})$ in physical space is simply

$$\frac{\partial T(\boldsymbol{x},t)}{\partial t} = -N^2 w(\boldsymbol{x},t). \tag{4.16}$$

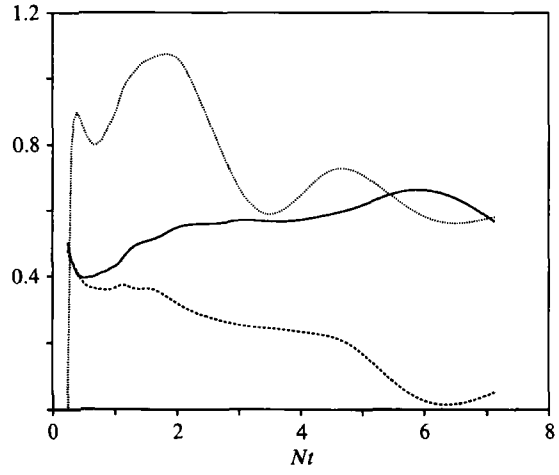

FIGURE 19. Time evolution (normalized by N) of the skewness factors $-S_{\partial u/\partial x}$ (——), $-S_{\partial w/\partial z}$ (– – – –), and $S_{\partial T/\partial z}$ (.....), stably stratified direct simulation.

Differentiating (4.16) with respect to z, we get

$$\frac{\partial}{\partial t}\left(\frac{\partial T}{\partial z}\right) = -N^2 \frac{\partial w}{\partial z}. \tag{4.17}$$

From (4.17) we get

$$\frac{1}{3}\frac{\langle(\partial T/\partial z)^3\rangle}{\partial t} = -N^2\left\langle\left(\frac{\partial w}{\partial z}\right)\left(\frac{\partial T}{\partial z}\right)^2\right\rangle. \tag{4.18}$$

We have

$$\langle(\partial w/\partial z)(\partial T/\partial z)^2\rangle = S_{Tw}[\langle(\partial w/\partial z)^2\rangle^{\frac{1}{2}}\langle(\partial T/\partial z)^2\rangle], \tag{4.19}$$

where S_{Tw} is the mixed-derivative skewness, found negative in our calculation. For isotropic turbulence, $-S_{Tw}$ is a measure of temperature-variance spectral transfer to large wavenumber (Herring & Kerr 1982; Kerr 1985). Therefore, $\langle(\partial T/\partial z)^3\rangle$ will grow to a positive finite value, and so will $S_{\partial T/\partial z}$. A more dynamical explanation is that locally large negative values of $\partial T/\partial z$ are convectively unstable and therefore rapidly destroyed by buoyancy forces, whereas large positive values enhance stability and therefore tend to persist. The skewness of the temperature fluctuation derivative in the direction of the mean temperature gradient was also found to be non-zero in the laboratory experiment by Sreenivasan & Antonia (1977). In the absence of mean shear, $S_{\partial T/\partial x}$ and $S_{\partial T/\partial y}$ (given in table 1) remain zero, as in the isotropic case (Sreenivasan & Tavoularis 1980).

Figure 19 shows the time evolution (normalized by N) of $-S_{\partial u/\partial x}$, $-S_{\partial w/\partial z}$ and $S_{\partial T/\partial z}$. Corresponding values for an isotropic velocity field are given in table 1 at $t_i = 17/v_0 k_i(0)$. The turbulence collapse is accompanied by a very strong decrease of $-S_{\partial w/\partial z}$. As pointed out by Riley *et al.* (1981), this indicates an inhibition by the stratification of the spectral energy transfer due to the $w\partial w/\partial z$ term in the momentum equation. By contrast, $-S_{\partial u/\partial x}$ increases with decreasing Froude number. In an initial phase, $S_{\partial T/\partial z}$ rises to very large values (≈ 1). It then decreases to catch up with the horizontal velocity derivative skewness. Figure 20 is the analogue of figure 19 for the large-eddy Boussinesq calculation presented in the previous section. For the three factors, the time-evolution is qualitatively similar to the previous case. However, in the direct numerical simulation, $-S_{\partial w/\partial z}$ drops to much smaller values during the collapsed phase.

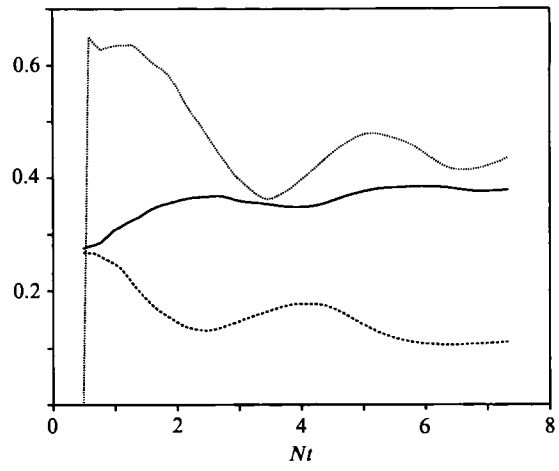

FIGURE 20. Same as figure 19 but for large-eddy simulation.

5. Eddy viscosity and diffusivity in physical space

Spectral large-eddy simulations neglecting ν_t^+ dependence on k have been performed at low resolution (32^3) by Chollet & Lesieur (1981) and have given acceptable results. The eddy viscosity (2.4) was replaced by

$$\nu_t(t) = \nu_t^+ \left[\frac{E(k_c, t)}{k_c}\right]^{\frac{1}{2}}, \tag{5.1}$$

with $\nu_t^+ = 0.267$ (for $C_k = 1.4$), the asymptotic value for $k \to 0$. However, in these calculations, the global drain of energy out of the large scales was found to be too weak and might have been improved with the use of the average eddy viscosity $\nu_t^{av}(t)$ defined by Leslie & Quarini (1979). Indeed, the energy balance in this case leads to (since the computed explicit energy transfer is conservative):

$$\int_0^{k_c} 2\nu_t^{av}(t)\, k^2 E(k, t)\, dk = \epsilon(t). \tag{5.2}$$

Hence, for an inertial-range Kolmogorov spectrum:

$$E(k) = C_k \epsilon^{\frac{2}{3}} k^{-\frac{5}{3}}, \tag{5.3}$$

with $C_k = 1.4$, (5.2) gives

$$\nu_t^{av} \left[\frac{E(k_c)}{k_c}\right]^{-\frac{1}{2}} = \tfrac{2}{3} C_k^{-\frac{3}{2}} \approx 0.402. \tag{5.4}$$

This constant is weakly influenced by the spectrum shape in the largest scales: the value derived from the kinetic energy spectrum of figure 1 is 0.38. This analysis can easily be extended to the eddy diffusivity (Antonopoulos-Domis 1981). The scalar variance conservation yields

$$\int_0^{k_c} 2\kappa_t^{av}(t)\, k^2 E_T(k, t)\, dk = \eta(t), \tag{5.5}$$

where η is the temperature-variance dissipation rate. Assuming a scalar spectrum which obeys Corrsin–Oboukhov's law

$$E_T(k) = C_{CO}\, \eta \epsilon^{-\frac{1}{3}} k^{-\frac{5}{3}}, \tag{5.6}$$

and a kinetic energy spectrum defined by (5.3), we get

$$Pr_t = \frac{\nu_t^{av}}{\kappa_t^{av}} = \frac{C_{CO}}{C_K}. \tag{5.7}$$

The Corrsin–Oboukhov constant was found to be close to 0.9 in the large-eddy simulation previously described. Consequently, in all the calculations presented in this section, the eddy Prandtl number will be taken equal to 0.6.

Neglecting the ν_t and κ_t dependence on k in (3.1) and (3.2), transforming back to physical space, and writing $\boldsymbol{u}(\boldsymbol{x}) = (u_1(\boldsymbol{x}), u_2(\boldsymbol{x}), u_3(\boldsymbol{x}))$ and $\boldsymbol{x} = (x_1, x_2, x_3)$, we get

$$\frac{\partial \bar{u}_i}{\partial t} = -\frac{1}{\rho}\frac{\partial \bar{P}}{\partial x_i} + \bar{u}_j \bar{\omega}_{ij} + \frac{\partial}{\partial x_j}\left\{(\nu+\nu_t)\left(\frac{\partial \bar{u}_i}{\partial x_j} + \frac{\partial \bar{u}_j}{\partial x_i}\right)\right\}, \tag{5.8}$$

$$\frac{\partial \bar{T}}{\partial t} = -\frac{\partial}{\partial x_j}\{\bar{u}_j \bar{T}\} + \frac{\partial}{\partial x_j}\left\{(\kappa+\kappa_t)\left(\frac{\partial \bar{T}}{\partial x_j}\right)\right\}, \tag{5.9}$$

$$\frac{\partial \bar{u}_j}{\partial x_j} = 0. \tag{5.10}$$

$\bar{a}(\boldsymbol{x})$ denotes the large-scale component of $a(\boldsymbol{x})$, which is given by a convolution of $a(\boldsymbol{x})$ with the filter function $G(\boldsymbol{x})$:

$$G(x_i) = \frac{2\sin(\pi x_i/\Delta x)}{\pi x_i}, \tag{5.11}$$

with

$$\Delta x = \pi/k_c. \tag{5.12}$$

The subgrid-scale part of the fields is $a' = a - \bar{a}$. $\bar{\omega}_{ij}$ is the vorticity tensor, $\bar{\omega}_{ij} = \partial \bar{u}_j/\partial x_i - \partial \bar{u}_i/\partial x_j$. $\bar{P}$ is a modified pressure determined with the aid of the continuity equation. When applying the filter directly to Navier–Stokes equations in physical space, with

$$R_{ij} - \tfrac{1}{3}\delta_{ij} R_{kk} = \nu_t(\partial \bar{u}_i/\partial x_j + \partial \bar{u}_j/\partial x_i),$$

R_{ij} being the total subgrid-scale Reynolds stress tensor $R_{ij} = -(\overline{\bar{u}_i u_j'} + \overline{u_i' \bar{u}_j} + \overline{u_i' u_j'})$, the set of equations (5.8), (5.10) is recovered with $\bar{P} = \bar{p}/\rho + \frac{1}{2}\bar{u}^2 + \frac{1}{3}R_{kk}$. The Leonard stress (Leonard 1974) is identically zero with the sharp filter.

These physical-space large-eddy simulation equations were originally formulated by Smagorinsky (1963) and Lilly (1967) and various approaches have been used for determining ν_t (see Voke & Collins 1983 for a review). An extensively used model is the one proposed by Smagorinsky (1963)

$$\nu_t(\boldsymbol{x}, t) = (C\Delta x)^2 \bar{S}^{\frac{1}{2}}, \tag{5.13}$$

with

$$\bar{S} = 2S_{ij}S_{ij}, \tag{5.14}$$

where S_{ij} is the *local* grid-scale strain-rate tensor

$$S_{ij} = \frac{1}{2}\left(\frac{\partial \bar{u}_i}{\partial x_j} + \frac{\partial \bar{u}_j}{\partial x_i}\right). \tag{5.15}$$

However, in order to determine the adjustable constant C in (5.13), the spatially fluctuating quantity $\bar{S}$ has to be replaced by its volume average $\langle \bar{S} \rangle$ (see e.g. Lilly 1967; Leslie & Quarini 1979) and consequently $\nu_t(\boldsymbol{x}, t)$ by $\nu_t^{av}(t)$. Thus, (5.2) can be used to express energy conservation. Furthermore, the energy dissipation can be written as (Lilly 1967)

$$\epsilon(t) = (C\Delta x)^2 \langle \bar{S}^{\frac{3}{2}} \rangle. \tag{5.16}$$

Using (5.2), (5.3), (5.13) and (5.16) gives

$$C = \frac{1}{\pi}\left(\frac{3C_{\mathrm{K}}}{2}\right)^{-\frac{3}{4}} \frac{\langle \bar{S} \rangle^{\frac{3}{2}}}{\langle \bar{S}^{\frac{3}{2}} \rangle}. \tag{5.17}$$

If the strain-rate ratio is assumed unity, evaluation of (5.17) indicates that $C \approx 0.2$.

The spectral eddy viscosity without a cusp, given by (5.1), can be employed in physical space. However, the eddy viscosity scales on $[E(k_{\mathrm{c}}, t)/k_{\mathrm{c}}]^{\frac{1}{2}}$, which averages all the velocity fluctuations on the computational domain. It is well known that turbulence is highly intermittent, with spatially localized vortical structures surrounded by quasi-irrotational fluid. In a calculation carried out in physical space, there is no need for any eddy-dissipation in the regions where the flow is calm. On the other hand, it is essential to dissipate in the subgrid scales the local bursts of turbulence if they become too intense. We thus propose to take an eddy viscosity varying in physical space, in the form

$$\nu_{\mathrm{t}}(\boldsymbol{x}|\Delta x) = \tfrac{2}{3} C_{\mathrm{K}}^{-\frac{3}{2}} \left(\frac{E_{\boldsymbol{x}}(k_{\mathrm{c}})}{k_{\mathrm{c}}}\right)^{\frac{1}{2}}, \tag{5.18}$$

where $E_{\boldsymbol{x}}(k_{\mathrm{c}})$ is a local kinetic energy spectrum at $\boldsymbol{x}$. How can we determine such a spectrum? As pointed out by Batchelor (1953) there is an obvious dualism between the Fourier coefficients and the velocity differences in physical space. We thus consider the local second-order velocity structure function

$$F_2(\boldsymbol{x}, \Delta x, t) = \langle \| \boldsymbol{u}(\boldsymbol{x}, t) - \boldsymbol{u}(\boldsymbol{x}+\boldsymbol{r}, t) \|^2 \rangle_{\|r\|=\Delta x} \tag{5.19}$$

(where $\langle . \rangle$ is an appropriate spatial average upon points $\boldsymbol{x}+\boldsymbol{r}$ a distance Δx from $\boldsymbol{x}$). It has been shown (Batchelor 1953) that, for isotropic turbulence,

$$F_2(r, t) = 4 \int_0^\infty E(k, t) \left[1 - \frac{\sin kr}{kr}\right] \mathrm{d}k. \tag{5.20}$$

For a spectrum of the form (5.3) extending from 0 to ∞, (5.20) yields (Orszag 1977)

$$F_2(r, t) = 4.82 C_{\mathrm{k}} (\epsilon r)^{\frac{2}{3}}, \tag{5.21}$$

which was the original formulation of Kolmogorov's law (Kolmogorov 1941).

Assuming that k_{c} lies in a Kolmogorov inertial range ($E(k_{\mathrm{c}})$ satisfies (5.3)), it follows from (5.21) that

$$E\left(\frac{\pi}{\Delta x}\right) = \frac{1}{4.82 \pi^{\frac{5}{3}}} \Delta x \, F_2(\Delta x, t). \tag{5.22}$$

Substituting into (5.18) yields

$$\nu_{\mathrm{t}}(\boldsymbol{x}|\Delta x) = 0.066 C_{\mathrm{k}}^{-\frac{3}{2}} \Delta x [F_2(\boldsymbol{x}, \Delta x, t)]^{\frac{1}{2}}. \tag{5.23}$$

If one chooses to evaluate the structure function at $r > \Delta x$, one can check that $\nu_{\mathrm{t}} \propto r F_2(r)^{\frac{1}{2}}$, the proportionality factor being $0.066 C_{\mathrm{k}}^{-\frac{3}{2}} (r/\Delta x)^{-\frac{4}{3}}$.

We now consider a large-eddy simulation of homogeneous isotropic turbulence carried out in physical space and we concentrate on the evaluation of $F_2(r)$. We can calculate the grid-scale structure function

$$\bar{F}_2(r) = \langle (\bar{\boldsymbol{u}}(\boldsymbol{x}+\boldsymbol{r}) - \bar{\boldsymbol{u}}(\boldsymbol{x}))^2 \rangle \tag{5.24}$$

and we have

$$F_2(r) = \bar{F}_2(r) + C_0(r, \Delta x) \tag{5.25}$$

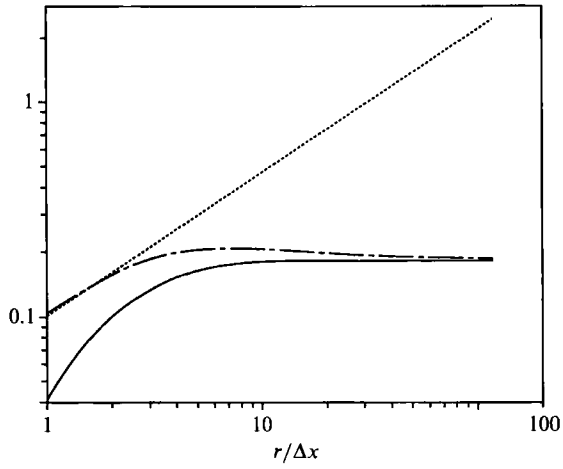

FIGURE 21. Velocity structure functions $\bar{F}_2(r)$ (——) and $F_2(r)$ (– – –) given by (5.30), evaluated in the calculation of figure 1. The dotted line shows the asymptotic value $F_2^a(r)$ given by (5.21). r is normalized by Δx.

where C_0 is the unknown contribution of the subgrid scales to the structure function. Its spectral expression is

$$C_0 = 4\int_{k_c}^{\infty} E(k,t)\left[1-\frac{\sin kr}{kr}\right]\mathrm{d}k. \tag{5.26}$$

We recall that k_c is related to Δx by (5.12). Assuming an inertial range extending from k_c to ∞, (5.26) yields

$$C_0(r,\Delta x) = F_2^a(r)\,(r/\Delta x)^{-\frac{2}{3}}H(r/\Delta x). \tag{5.27}$$

$F_2^a(r)$ is the asymptotic function given by (5.21) and $H(\zeta)$ has the following analytical expression:

$$H(\zeta) = \frac{4}{4.82}\int_{\pi}^{\infty}\delta'^{-\frac{5}{3}}\left[1-\frac{\sin\delta'\zeta}{\delta'\zeta}\right]\mathrm{d}\delta' = \frac{4}{4.82}\left[\tfrac{3}{2}\pi^{-\frac{2}{3}}-\zeta^{\frac{2}{3}}\int_{\zeta\pi}^{\infty}\delta'^{-\frac{8}{3}}\sin\delta'\,\mathrm{d}\delta'\right]. \tag{5.28}$$

From Gradshteyn & Ryzhik (1965), one gets

$$\int_{\zeta\pi}^{\infty}\delta'^{-\frac{8}{3}}\sin\delta'\,\mathrm{d}\delta' = \tfrac{1}{2}\mathrm{i}[\mathrm{e}^{-\pi/2\mathrm{i}(-\frac{5}{3})}\Gamma(-\tfrac{5}{3},\mathrm{i}\zeta\pi)-\mathrm{e}^{\pi/2\mathrm{i}(-\frac{5}{3})}\Gamma(-\tfrac{5}{3},-\mathrm{i}\zeta\pi)], \tag{5.29}$$

where Γ is the gamma function.

Replacing $F_2^a(r)$ by $F_2(r)$ in (5.26), we finally obtain the following physical-space estimation of $F_2(r)$:

$$F_2(r) = \left(\frac{1}{1-(r/\Delta x)^{-\frac{2}{3}}H(r/\Delta x)}\right)\bar{F}_2(r), \tag{5.30}$$

which allows one to determine the total structure function from the filtered signal.

Turning back to the large-eddy simulation of §3.1, figure 21 shows, at the end of the run, $\bar{F}_2(r)$ (computed in spectral space with the integral in (5.20) extending from 0 to k_c), $F_2(r)$ given by (5.30), and $F_2^a(r)$. r is normalized by Δx. We can see that it is only for $r \to \Delta x$ that the corrected structure function $F_2(r)$ collapses on the asymptotic

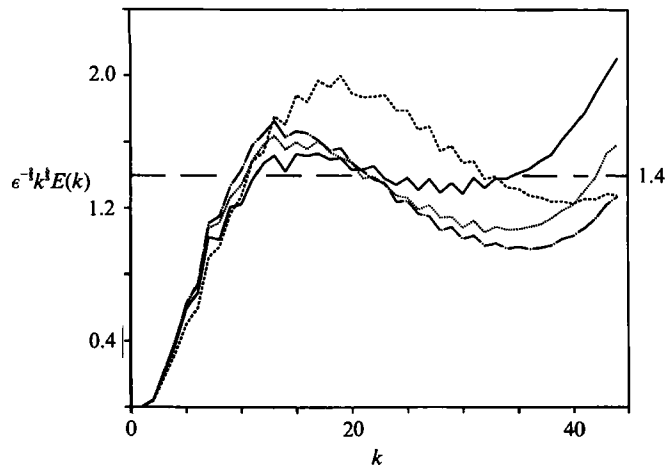

FIGURE 22. Compensated spectra $\epsilon^{-\frac{2}{3}}k^{\frac{5}{3}}E(k)$ in a large-eddy simulation (96^3 resolution points) with the physical-space eddy viscosity given by (5.32) (——). ($t = 22/v_0 k_1(0)$; $k_1(0) = 8$.) It is compared to the spectra obtained with spectral eddy viscosity given by $\nu_t(k|k_c, t) = \nu_t^+(k/k_c)[E(k_c, t)/k_c]^{\frac{1}{2}}$: k-dependent ν_t^+ (see (2.5)) (– – – –); constant $\nu_t^+ = 0.4$ (.....); —·—, Smagorinsky's model (see (5.13)) with $C = 0.2$.

determination corresponding to a Kolmogorov cascade extending to infinitely small scales. We notice also that, in this practical case, the correction proposed by (5.30) seems to work quite well.

If one considers inhomogeneous or highly intermittent flows, the former analysis can be valid if the subgrid scales and the smallest grid scales are locally homogeneous. One assumes that the large-scale inhomogeneities are directly taken into account by the simulation of the large scales themselves. In physical space, one can then estimate locally at each grid point (located at $\boldsymbol{x}$) the filtered structure function $\bar{F}_2(\boldsymbol{x}, r, t)$ by averaging over a sphere of radius r centred in $\boldsymbol{x}$. In practical cases, one takes $r = \Delta x$. For a regular cubic mesh in physical space, the local structure function is thus determined at each point by averaging over the six closest surrounding points. The total structure function $F_2(\boldsymbol{x}, \Delta x, t)$ can then be deduced from $\bar{F}_2(\boldsymbol{x}, \Delta x, t)$ through (5.30), which gives (for $r = \Delta x$):

$$F_2(\boldsymbol{x}, \Delta x, t) = 2.53 \times \bar{F}_2(\boldsymbol{x}, \Delta x, t). \tag{5.31}$$

Finally, (5.23) and (5.31) allow the determination of the local eddy viscosity:

$$\nu_t(\boldsymbol{x}, t) = 0.105 C_K^{-\frac{3}{2}} \Delta x [\bar{F}_2(\boldsymbol{x}, \Delta x, t)]^{\frac{1}{2}}. \tag{5.32}$$

For $C_K = 1.4$, the multiplying factor ≈ 0.063. This new model will be designated the *structure-function model*.

We have used the formulation (5.32) in an homogeneous isotropic calculation (96^3 collocation points) where the intermittent behaviour may render the use of the spatially varying eddy viscosity necessary. Pseudo-spectral methods are still used, but the dissipative term for the ith component of the velocity field $(\nu + \nu_t(k|k_c))\, k^2 \hat{u}_i$ is replaced in (3.1) by

$$\Pi\{k_j F[(\nu + \nu_t(\boldsymbol{x}))\, F^{-1}(k_j \hat{u}_i + k_i \hat{u}_j)]\}. \tag{5.33}$$

The compensated energy spectrum $\epsilon^{-\frac{2}{3}}k^{\frac{5}{3}}E(k)$ obtained with this physical-space subgrid-scale model at $t = 22/v_0 k_1(0)$ ($k_1(0) = 8$) is shown in figure 22. It is compared to the spectra obtained with spectral eddy viscosity given by $\nu_t(k|k_c, t) =$

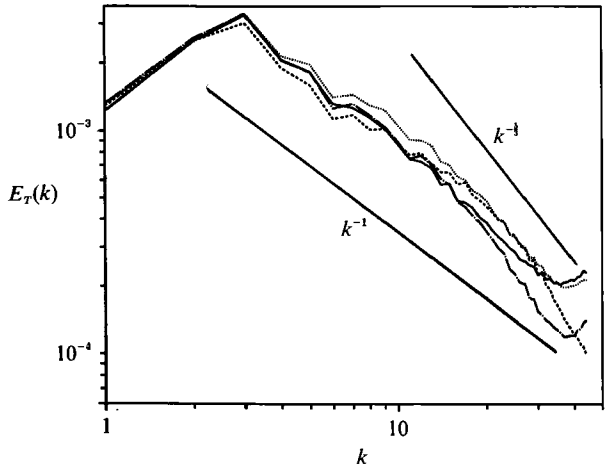

FIGURE 23. Scalar spectra corresponding to the calculation of figure 22.

$\nu_t^+(k/k_c)\,[E(k_c,t)/k_c]^{\frac{1}{2}}$, first with ν_t^+ dependency on k given by (2.5), secondly ignoring k-dependency and taking $\nu_t^+ = 0.4$. The spectrum given by a simulation using spatially fluctuating Smagorinsky's eddy viscosity (see (5.13)) is also plotted. Except for the spectral region near the cutoff, where the dissipation is underestimated, the spectrum, as given by the physical-space structure function model exhibits a long spectral range of slope $\approx -\frac{5}{3}$ (with a Kolmogorov constant $C_k \approx 1.4$). This is an improvement compared to the calculations with spectral eddy viscosity (which yield an inertial spectrum closer to k^{-2}). In the same way, the Smagorinsky model gives excessively steep decay of the energy spectrum at large wavenumber, indicating that it dissipates too much energy from the resolved scales. Similar results were noticed in the large-eddy simulation of turbulent channel flows performed by Piomelli, Moin & Ferziger (1988). The passive-scalar spectrum obtained with the structure function model displays a well-defined $\approx k^{-1}$ spectral range up to $k \approx k_c$ (figure 23). This spectrum is very close to the one given by the Smagorinsky model, except at high wavenumbers. The differences observed at all wavenumbers with the spectra resulting from simulations with spectral eddy viscosity could be because spatially varying eddy diffusivities take better account of scalar strong intermittency, although we have checked that the various p.d.f.s do not depend very much on the subgrid-scale model used. At large scales, the kinetic energy spectrum obtained with the structure function model is in good agreement with that of direct numerical simulation with 128^3 collocation points presented in §3.2 (figure 24*a*). However, the best agreement for the large-scale scalar variance is achieved when numerical simulations are performed with a molecular Prandtl number equal to the turbulent one: $Pr = 0.6$ (see figure 24*b*). The large scales of the flow do not seem to distinguish between molecular and turbulent diffusion coefficients, at least in the early phase of the decay.

5.1. *Flow structures*

Vorticity structures in three-dimensional homogeneous isotropic turbulence have been extensively studied (see e.g. Siggia & Patterson 1978; Siggia 1981; Yamamoto & Hosokawa 1988; She, Jackson & Orszag 1990; Vincent & Meneguzzi 1991). Numerical results show that high-vorticity-amplitude regions are associated with tube-like objects. Several investigators have been studying strong vortical regions

(*a*)

(*b*)

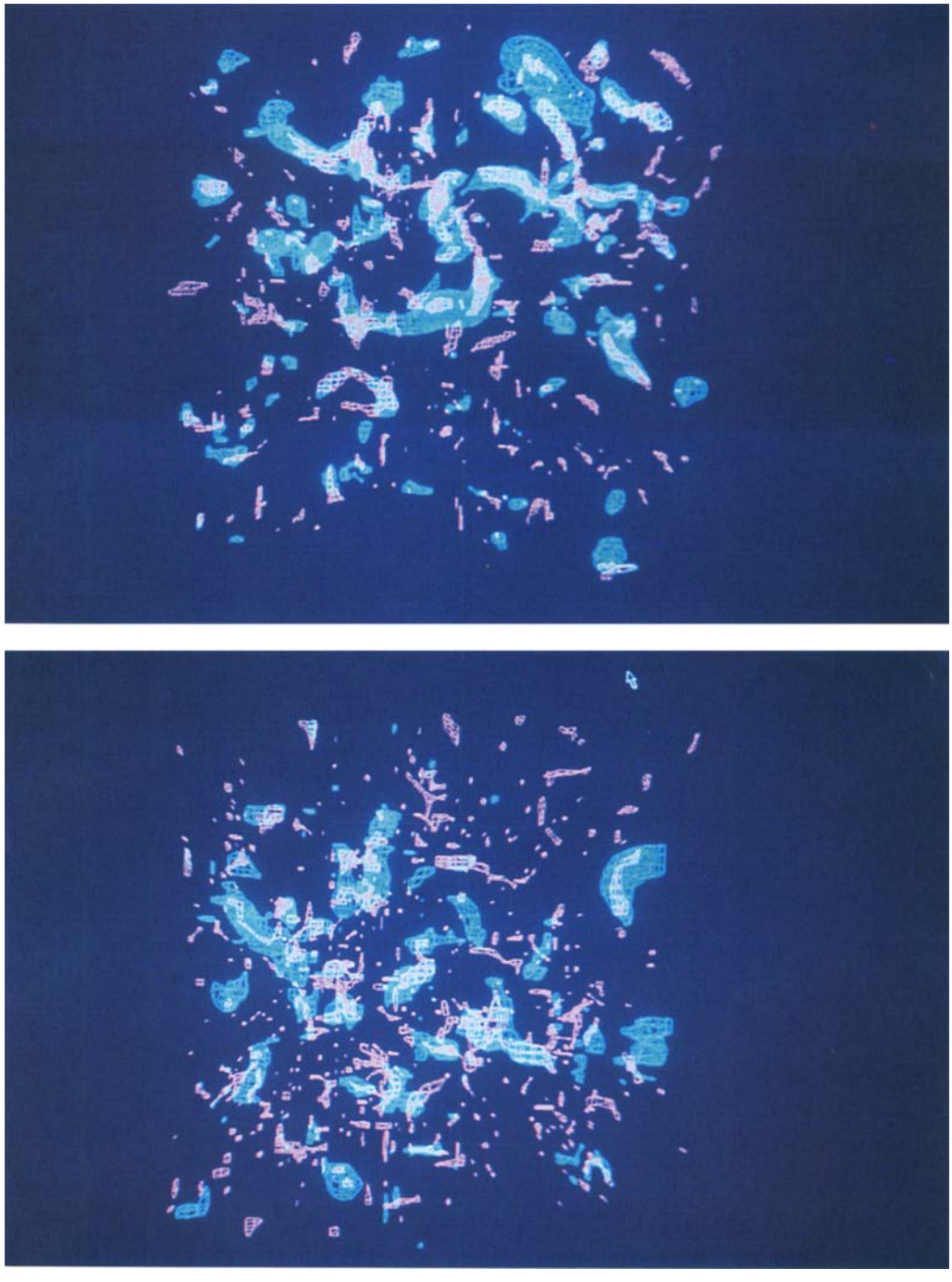

FIGURE 25. (*a*) Direct numerical simulation (128^3 resolution points), (*b*) large-eddy simulation with the structure function subgrid-scale model (96^3 resolution points). The red surfaces bound the regions within which the vorticity modulus $|\omega| = (\omega^2)^{1/2}$ is larger than a given percentage of the instantaneous maximum: 42% for (*a*) and 55% for (*b*). The blue surfaces delimit regions where the pressure p verifies $p_{min} \leq p \leq 0.42\, p_{min}$; p_{min} is the instantaneous pressure minimum ($p_{min} < 0$).

(*Facing p.* 186)

FIGURE 26. Direct numerical simulation (128^3 resolution points) corresponding to figure 25(*a*). The blue surfaces delimit regions where the pressure p verifies $p_{min} \leq p \leq 0.36\, p_{min}$. The green surfaces bound the regions within which the absolute value of the scalar fluctuations is larger than 41% of the instantaneous maximum.

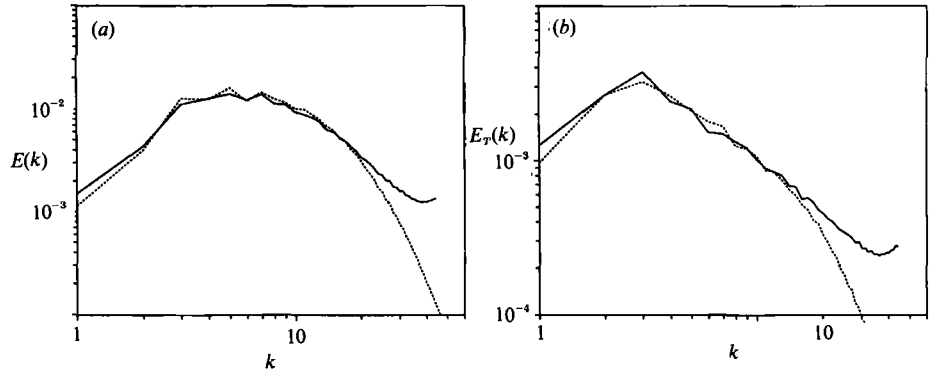

FIGURE 24. (*a*) Comparison of the kinetic energy spectra obtained with the structure function model with 96^3 collocation points (——) and in a direct numerical simulation with 128^3 points (.....). In both cases, $t = 21/v_0 k_1(0)$; $k_1(0) = 8$. (*b*) Corresponding scalar spectra. The molecular Prandtl number for the direct numerical simulation is equal to the eddy Prandtl number used in the large-eddy simulation: $Pr = 0.6$.

using other criteria such as low pressure (e.g. Wray & Hunt 1990; Brachet 1990; Silveira-Neto *et al.* 1991). We focus here on the comparison between the turbulent structures given by the direct numerical simulation of §3.2 shown in figure 25(*a*) (plate 1) and by the large-eddy simulation using the structure function model shown in figure 25(*b*) (plate 1). The red pink surfaces bound the regions within which the vorticity modulus $|\omega| = (\omega^2)^{\frac{1}{2}}$ is larger than a given percentage of the instantaneous maximum: 42% for figure 25(*a*) and 55% for figure 25(*b*). The pressure can be determined through the Poisson equation except for an additive constant. The constant is chosen here such that the pressure volume average is zero: the low-pressure regions thus correspond to negative values, high pressure to positive ones. For figures 25(*a*) and 25(*b*), the blue surfaces delimit regions where the pressure p verifies $p_{\min} \leqslant p \leqslant 0.42 p_{\min}$, where $p_{\min}$ is the instantaneous pressure minimum ($p_{\min} < 0$). In both cases, $\frac{1}{8}$th of the computational domain is represented. In the case of the direct numerical simulation (figure 25*a*), three-dimensional plots of the vorticity reveal elongated, 'worm-like' structures. These structures correlate well with the low-pressure ones. As in Vincent & Meneguzzi (1991), the length of these objects is of the order of the integral scale, while their diameter corresponds to inertial-range scales. As already shown above in figures 5(*f*) and 5(*g*), our pressure p.d.f.s exhibit a very asymmetric shape, with a remarkable exponential fit in the low regions, when while the high-pressure one is very close to Gaussian. This constitutes another signature of strong vortical concentration. The corresponding skewness factor is ≈ -1.0. Figure 25(*b*) indicates that concentrated low-pressure structures are still present in large-scale simulations. They are elongated and correlated to some of the vorticity structures. However, the high-vorticity regions are very scattered due to the high vorticity level in the smallest resolved scales. Therefore, the low-pressure structures are better tracers of the coherent structures.

We present in figure 26 (plate 2) (direct numerical simulation) the low-pressure (blue) and high-temperature fluctuations (green). It is striking that temperature is stretched in the 'braid' region between the large billows. This is reminiscent of two-dimensional turbulence, and might confirm the enstrophy cascading-type cascade proposed above to explain the anomalous k^{-1} temperature spectrum.

Finally, we have plotted, for the simulation based on the structure-function model,

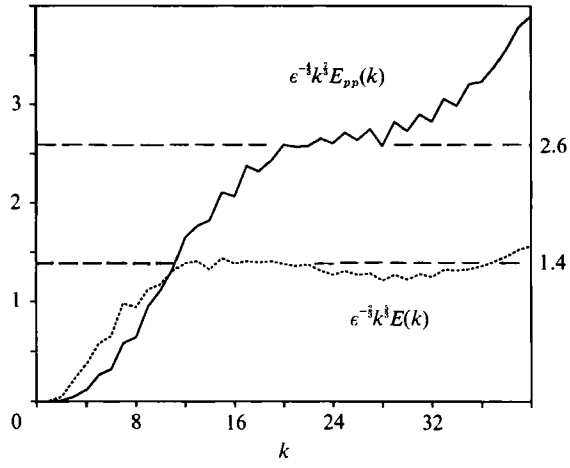

FIGURE 27. Compensated pressure (——) and kinetic energy (– – –) spectra for the structure-function model based simulation corresponding to figure 22.

the pressure spectrum compensated following Oboukhov's (1949) and Batchelor's (1951) quasi-normal predictions in a Kolmogorov kinetic energy cascade:

$$E_{pp}(k) = \alpha C_k^2 \epsilon^{\frac{4}{3}} k^{-\frac{7}{3}}. \tag{5.34}$$

The constant α may be determined from Monin & Yaglom (1975) as

$$\alpha = \frac{7}{3}\left(\frac{27}{55}\right)^2 \frac{\Gamma(\frac{1}{3})^2}{\Gamma(-\frac{4}{3})} \approx 1.32. \tag{5.35}$$

This constant was also given by Georges, Beuther & Arndt (1984). Figure 27 shows the compensated spectrum $\epsilon^{-\frac{1}{3}}k^{\frac{7}{3}}E_{pp}$, which is compared with the corresponding kinetic energy spectrum compensated by Kolmogorov's law. We notice that Batchelor's law seems to be valid for $k > 20$ (the high-k cusp being certainly a contamination due to the inadequate representation of the velocity at k_c), with a proportionality constant $\approx 2.6 = 1.32 C_k^2$ in very good agreement with the theoretical prediction. The same spectral behaviour with a constant of the same order has been obtained for the pressure by Fung *et al.* (1992) using a method based on kinematic simulations. Therefore, the pressure-variance spectrum decreases at large wavenumber more rapidly than the kinetic energy spectrum, so that the contribution of the small-scale motions is much less important for the pressure fluctuations than for the velocity fluctuations. This remark is even truer when comparing pressure and vorticity fluctuations.

5.2. *Further applications of the structure-function model*

In addition to the case of isotropic incompressible turbulence, the structure function model has also been respectively applied to the incompressible flow behind a backward-facing step (Silveira Neto *et al.* 1991) and to a high-supersonic boundary layer (Mach 5) spatially developing above a flat plate (Normand & Lesieur 1991). These studies showed that the model presents the double advantage of allowing the vortex coherent structures of the flow to develop, and of predicting accurately the flow statistics. In the case of the step, intense longitudinal hairpin vortices are found and the computed flow statistics are in good agreement with those measured in the

laboratory experiments performed by Eaton & Johnston (1980). For the compressible boundary layer at Mach 5, Λ-shaped vortices staggered in the spanwise direction form, in the case of forced transition. The structure resembles the staggered mode proposed by Herbert (1988) in the incompressible boundary layer, for the natural transition case. This illustrates the intense three-dimensionalizing effect of compressibility. Notice also that no direct numerical simulation is possible at high Mach number, owing to the high critical Reynolds number. Therefore, the LES is the only possible approach for deterministic simulation in this case.

6. Conclusion and discussion

In the spectral large-eddy and direct numerical simulations of decaying turbulence described here, a convected passive scalar displays several *anomalous* characteristics: a k^{-1} spectrum in the large scales; $\ln k$ eddy diffusivity; large-scale intermittency with exponential probability density functions; decay laws much stronger than the ones predicted by statistical theories of turbulence or observed in some grid-turbulence experiments.

The coupling between temperature and velocity fields due to the presence of stable stratification greatly modifies the temperature behaviour. The average decay rate for the available potential energy is now comparable to the 'turbulent' velocity component decay rate. The former no longer displays the anomalous spectral behaviour it had in the isotropic case and the eddy Prandtl number is ≈ 0.45 at all wavenumbers. The temperature fluctuation exhibits a Gaussian distribution. Large differences in the degree of intermittency between the passive and non-passive cases are confirmed by the oceanic measurements of Gargett (1985). Furthermore, the clear difference between temperature distribution histograms when the latter is passive and when buoyancy forces are present could indicate regimes of *hard* and *soft* turbulence similar to those observed in Rayleigh–Bénard convection by Castaing *et al.* (1989). The most striking feature of the temperature-fluctuation field is the strong skewness of its derivative in the direction of the mean temperature gradient. This has been observed in several laboratory experiments and seems to be attributable to the buoyancy term in the temperature equation. We have distinguished between *pre-collapse* and *post-collapse* phases during the decay of the stratified turbulence. In the former stage, the Froude number is large and the 'turbulent' component of the velocity field is weakly affected by the buoyancy forces, and the eddy-viscosity coefficients are the same as in the isotropic case. The latter stage (small-Froude-number regime) is characterized by an inhibition of the spectral transfers towards small scales implying a weaker dissipation and a reduction in the estimated eddy coefficients. Differences between eddy-viscosity coefficients for the 'vortex' and the 'wave' components of the velocity field could suggest some improvements in the subgrid-scale modelling. Furthermore, angular dependency of the eddy coefficients versus wavenumbers has to be investigated. In the collapsed state, the vertical velocity longitudinal derivative skewness becomes very small.

We have also proposed a new formulation of the eddy-viscosity coefficient in physical space derived directly from Chollet & Lesieur's (1981) spectral formulation, where the kinetic energy spectrum is calculated with the aid of a local second-order velocity structure function. From the explicitly calculated large scales, we can only estimate a truncated structure function. We propose here a correction which allows us to determine the total structure function from the filtered signal. We have called the result the *structure-function model.*

The subgrid-scale parameterization proposed here is valid as long as the subgrid scales and the smallest explicit scales are locally isotropic and homogeneous. This does not represent too big a constraint if the large-scale inhomogeneities are correctly described by the explicit calculation: spectral homogeneous and isotropic subgrid-scale modelling by Chollet & Lesieur (1981) has been applied by Comte *et al.* (1990) to the large-eddy simulation of free-shear layers. Their simulation showed the appearance of longitudinal vortices, and also velocity fluctuations levels in excellent agreement with those found in the laboratory experiments.

Contrary to the spectral one, the physical-space eddy-viscosity of the structure function model can be estimated locally in space: this is important for intermittent flows where the use of spatially varying eddy viscosity may be necessary. Our present study shows that the structure function model gives good results in the case of homogeneous isotropic turbulence, where internal intermittency exists, as the numerical calculations indicate. By comparison with spectral models and with Smagorinsky's model, the new one gives the best agreement with the $k^{-\frac{5}{3}}$ Kolmogorov kinetic energy spectrum, with a Kolmogorov constant $C_k \approx 1.4$. Comparisons with high-resolution direct simulations show a good concordance at large scale. In both cases, the pressure probability function exhibits a very asymmetric shape with a remarkable exponential fit in the low-pressure wing. This reveals the presence of localized low-pressure structures as confirmed on the three-dimensional pressure plots. On the other hand, the high-vorticity regions, as given by the large-eddy simulations, are very scattered and much less correlated to the low-pressure areas than in the case of direct simulations. This indicates that low-pressure regions are the best tracer of areas of turbulent activity when only the largest scales of the flow are simulated. Finally, we have checked that Batchelor's $k^{-\frac{7}{3}}$ quasi-normal law for the pressure spectrum is valid within the Kolmogorov range, and have determined the universal constant of this pressure spectrum, found of the order of $1.32C_k^2$.

As shown in other calculations, the structure function model can be applied successfully to separated flows behind a backward-facing step and high-supersonic boundary layer above a flat plate. The model is able to both allow for the development of the vortex coherent structures and to give an accurate prediction of the flow statistics.

We are grateful to P. Comte, J. R. Herring, J. J. Riley and A. Silveira Neto for many fruitful discussions. We also thank E. David who was of great assistance in the programming development. We are indebted to the referees for extremely constructive comments. Computations were carried out at the CCVR (Centre de Calcul Vectoriel pour la Recherche). This work was supported by the CNRS (GRD 'Mécanique des Fluides Numérique') and by the DRET (contract 87/238).

REFERENCES

André, J. C. & Lesieur, M. 1977 Influence of helicity on the evolution of isotropic turbulence at high Reynolds number. *J. Fluid Mech.* **81**, 187–207.

Anselmet, F., Gagne, Y., Hopfinger, E. J. & Antonia, R. A. 1984 High-order velocity structure functions in turbulent shear flows. *J. Fluid Mech.* **140**, 63–89.

Antonia, R. A., Chambers, A. J., Van Atta, C. W., Friehe, C. A. & Helland, K. N. 1978 Skewness of temperature derivative in a heated grid flow. *Phys. Fluids* **21**, 509–510.

Antonia, R. A., Hopfinger, E. J., Gagne, Y. & Anselmet, F. 1984 Temperature structure functions in turbulent shear flows. *Phys. Rev.* A **30**, 2704–2707.

ANTONIA, R. A., RAJAGOPALAN, S., BROWNE, L. W. B. & CHAMBERS, A. J. 1982 Correlations of squared velocity and temperature derivatives in a turbulent plane jet. *Phys. Fluids* **25**, 1156–1158.

ANTONOPOULOS-DOMIS, M. 1981 Large-eddy simulation of a passive scalar in isotropic turbulence. *J. Fluid Mech.* **104**, 55–79.

BATCHELOR, G. K. 1951 Pressure fluctuations in isotropic turbulence. *Proc. Camb. Phil. Soc.* **47**, 359–374.

BATCHELOR, G. K. 1953 *The Theory of Homogeneous Turbulence.* Cambridge University Press, 197 pp.

BATCHELOR, G. K. 1959 Small scale variation of convected quantities like temperature in turbulent fluid. Part 1. General discussion and the case of small conductivity. *J. Fluid Mech.* **5**, 113–134.

BATCHELOR, G. K., CANUTO, V. M. & CHASNOV, J. R. 1992 Homogeneous buoyancy generated turbulence. *J. Fluid Mech.* **235**, 349–378.

BÈGUE, C., CHACÓN, T., ORTEGÓN, F. & PIRONNEAU, O. 1987 3D simulation of 2 length scales turbulent flows by homogenization. In *Advances in Turbulence 1* (ed. G. Comte-Bellot & J. Mathieu), pp. 135–142. Springer.

BRACHET, M. 1990 Géométrie des structures à petite échelle dans le vortex de Taylor–Green. *C.R. Acad. Sci. Paris* II **311**, 775–780.

CAMBON, C. 1989 Spectral approach to axisymmetric turbulence in a stratified fluid. In *Advances in Turbulence 2* (ed. H. H. Fernholtz & H. E. Fiedler), pp. 162–167. Springer.

CAMBON, C. & JACQUIN, L. 1989 Spectral approach to non-isotropic turbulence subjected to rotation. *J. Fluid Mech.* **202**, 295–317.

CASTAING, B., GAGNE, Y. & HOPFINGER, E. J. 1990 Velocity probability density functions of high Reynolds number turbulence. *Physica* D **46**, 177–200.

CASTAING, B., GUNARATNE, G., HESLOT, F., KADANOFF, L., LIBCHABER, A., THOMAE, S., WU, X.-Z., ZALESKI, S. & ZANETTI, G. 1989 Scaling of hard thermal turbulence in Rayleigh–Bénard convection. *J. Fluid Mech.* **204**, 1–30.

CHOLLET, J.-P. 1984 Turbulence tridimensionnelle isotrope: modélisation statistique des petites échelles et simulation numérique des grandes échelles. Thèse de Doctorat d'État, Grenoble.

CHOLLET, J.-P. 1985 Two-point closure used for a sub-grid scale model in large eddy simulations. In *Turbulent Shear Flows 4* (ed. L. J. S. Bradbury *et al.*), pp. 62–72. Springer.

CHOLLET, J.-P. & LESIEUR, M. 1981 Parameterization of small scales of three-dimensional isotropic turbulence utilizing spectral closures. *J. Atmos. Sci.* **38**, 2747–2757.

COMTE, P., LESIEUR, M. & FOUILLET, Y. 1990 Coherent structures of mixing layers in large-eddy simulation. In *Topological Fluid Mechanics* (ed. H. K. Moffatt & A. Tsinober), pp. 649–658. Cambridge University Press.

CORRSIN, S. 1964 The isotropic turbulent mixer: Part II. Arbitrary Schmidt number. *AIChE J.* **18**, 417–423.

CRAYA, A. 1958 *Contribution à l'Analyse de la Turbulence Associée à des Vitesses Moyennes.* P. S. T. Ministère de l'Air, 345 pp.

DOMARADZKI, J. A., METCALFE, R. W., ROGALLO, R. S. & RILEY, J. J. 1987 Analysis of subgrid-scale eddy viscosity with the use of results from direct numerical simulations. *Phys. Rev. Lett.* **58**, 547–550.

EATON, J. K. & JOHNSTON, J. P. 1980 *Stanford Rep.* MD 39.

FOURNIER, J.-D. 1977 Quelques méthodes systématiques de développement en turbulence homogène. Thèse, Université de Nice.

FUNG, J. C. H., HUNT, J. C. R., MALIK, N. A. & PERKINS, R. J. 1992 Kinematic simulation of homogeneous turbulence by unsteady random Fourier modes. *J. Fluid Mech.* **236**, 281–317.

GAGNE, Y. 1987 Etude expérimentale de l'intermittence et des singularités dans le plan complexe en turbulence développée. Thèse, Université de Grenoble.

GARGETT, A. E. 1985 Evolution of scalar spectra with the decay of turbulence in a stratified fluid. *J. Fluid Mech.* **159**, 379–407.

GEORGES, W. K., BEUTHER, P. D. & ARNDT, R. E. A. 1984 Pressure spectra in turbulent free shear flows. *J. Fluid Mech.* **148**, 155–191.

GRADSHTEYN, I. S. & RYZHIK, I. M. 1965 *Table of Integrals Series and Products.* Academic.

HERBERT, T. 1988 Secondary instability in boundary layers. *Ann. Rev. Fluid Mech.* **20**, 487–526.

HERRING, J. R. 1974 Approach of axisymmetric turbulence to isotropy. *Phys. Fluids* **17**, 859–872.

HERRING, J. R. 1990 Comparison of closure to the spectral-based large eddy simulations. *Phys. Fluids* **2**, 979–983.

HERRING, J. R. & KERR, R. M. 1982 Comparison of direct numerical simulations with predictions of two-point closures for isotropic turbulence convecting a passive scalar. *J. Fluid Mech.* **118**, 205–219.

HERRING, J. R., SCHERTZER, D., LESIEUR, M., NEWMANN, G. R., CHOLLETT, J.-P. & LARCHEVÊQUE, M. 1982 A comparative assessment of spectral closures as applied to passive scalar diffusion. *J. Fluid Mech.* **124**, 411–437.

HUNT, J. C. R. & VASSILICOS, J. C. 1991 Kolmogorov's contributions to the physical and geometrical understanding of small-scale turbulence and recent developments. *Proc. R. Soc. Lond.* A **434**, 183–210.

KAIMAL, J. C., WYNGAARD, J. C., IZUMI, Y. & COTÉ, O. R. 1972 Spectral characteristics of surface-layer turbulence. *Q. J. R. Met. Soc.* **98**, 563–589.

KERR, R. M. 1985 Higher-order derivative correlations and the alignment of small-scale structures in isotropic numerical turbulence. *J. Fluid Mech.* **153**, 31–58.

KOLMOGOROV, A. N. 1941 The local structure of turbulence in incompressible viscous fluid for very large Reynolds number. *Dokl. Akad. Nauk SSSR* **30**, 301–305.

KOLMOGOROV, A. N. 1962 A refinement of previous hypotheses concerning the local structure of turbulence in a viscous incompressible fluid at high Reynolds number. *J. Fluid Mech.* **12**, 82–85.

KRAICHNAN, R. H. 1966 Isotropic turbulence and inertial-range structure. *Phys. Fluids* **9**, 1728–1752.

KRAICHNAN, R. H. 1968 Small-scale structure of a scalar field convected by turbulence. *Phys. Fluids* **11**, 945–953.

KRAICHNAN, R. H. 1976 Eddy viscosity in two and three dimensions. *J. Atmos. Sci.* **33**, 1521–1536.

KRAICHNAN, R. H. 1990 Models of intermittency in hydrodynamic turbulence. *Phys. Rev. Lett.* **65**, 575–578.

LEE, T. D. 1952 On some statistical properties of hydrodynamical and magneto hydrodynamical fields. *Q. Appl. Maths* **10**, 69–74.

LEONARD, A. 1974 Energy cascade in large-eddy simulations of turbulent fluid flows. *Adv. Geophys.* A **18**, 237–248.

LESIEUR, M. 1987 *Turbulence in Fluids.* Nijhoff. 286 pp.

LESIEUR, M. 1990 *Turbulence in Fluids* (revised edn). Kluwer. 412 pp.

LESIEUR, M., MÉTAIS, O. & ROGALLO, R. S. 1989 Etude de la diffusion turbulente par simulation des grandes échelles. *C.R. Acad. Sci. Paris* II **308**, 1395–1400.

LESIEUR, M., MONTMORY, C. & CHOLLET, J.-P. 1987 The decay of kinetic energy and temperature variance in three-dimensional isotropic turbulence. *Phys. Fluids* **30**, 1278–1286.

LESIEUR, M. & ROGALLO, R. S. 1989 Large-eddy simulation of passive scalar diffusion in isotropic turbulence. *Physics Fluids* A **1**, 718–722.

LESIEUR, M. & SCHERTZER, D. 1978 Amortissement auto similaire d'une turbulence à grand nombre de Reynolds. *J. Méc.* **17**, 609–646.

LESLIE, D. C. & QUARINI, G. L. 1979 The application of turbulence theory to the formulation of subgrid modelling procedures. *J. Fluid Mech.* **91**, 65–91.

LIGHTHILL, J. 1978 *Waves in Fluids.* Cambridge University Press, 504 pp.

LILLY, D. K. 1967 The representation of small-scale turbulence in numerical simulation experiments. *Proc. IBM Sci. Comput. Symp. Environ. Sci., IBM Data Process. Div., White Plains, NY*, pp. 195–210.

LILLY, D. K. 1983 Stratified turbulence and the mesoscale variability of the atmosphere. *J. Atmos. Sci.* **40**, 749–761.

McWILLIAMS, J. C. 1989 Statistical properties of decaying geostrophic turbulence. *J. Fluid Mech.* **198**, 199–230.

MESTAYER, P. 1982 Local isotropy in a high-Reynolds-number turbulent boundary layer. *J. Fluid Mech.* **125**, 475–503.

MÉTAIS, O. & CHOLLET, J.-P. 1989 Turbulence submitted to stable density stratification: large-eddy simulations and statistical theory. *Turbulent Shear Flows 6* (ed. J.-C. André *et al.*), pp. 398–415. Springer.

MÉTAIS, O. & HERRING, J. R. 1989 Numerical simulations of freely evolving turbulence in stably stratified fluids. *J. Fluid Mech.* **202**, 117–148.

MÉTAIS, O. & LESIEUR, M. 1986 Statistical predictability of decaying turbulence. *J. Atmos. Sci.* **43**, 857–870.

MÉTAIS, O. & LESIEUR, M. 1989 Large eddy simulations of isotropic and stably-stratified turbulence. In *Advances in Turbulence 2* (ed. H. H. Fernholz & H. E. Fiedler), pp. 371–376. Springer.

MONIN, A. S. & YAGLOM, A. M. 1975 *Statistical Fluid Mechanics*, Vol. 2, MIT Press.

NORMAND, X. & LESIEUR, M. 1991 Numerical experiments on transition in the compressible boundary layer over an insulated plate. *Theor. Comp. Fluid Dyn.* (in press).

OBOUKHOV, A. M. 1949 Pressure fluctuations in a turbulent flow. *Dokl. Akad. Nauk SSSR* **66**, 17–20.

ORSZAG, S. A. 1977 Lectures on the statistical theory of turbulence. In *Fluid Dynamics* (ed. R. Balian & J.-L. Peube), Les Houches, Juillet 1973, pp. 235–374. Gordon and Breach.

ORSZAG, S. A. & PATTERSON, G. S. 1972 Numerical simulation of turbulence. In *Statistical Models and Turbulence* (ed. M. Rosenblatt & C. Van Atta). Lecture Notes in Physics, Vol. 12, pp. 127–147. Springer.

PIOMELLI, U., MOIN, P. & FERZIGER, J. 1988 Model consistency in large eddy simulation of turbulent channel flows. *Phys. Fluids* **31**, 1884–1891.

RILEY, J. J., METCALFE, R. W. & WEISSMAN, M. A. 1981 Direct numerical simulations of homogeneous turbulence in density stratified fluids. In *Proc. AIP Conf. on Nonlinear Properties of Internal Waves* (ed. B. J. West), pp. 79–112.

ROGALLO, R. S. & MOIN, P. 1984 Numerical simulation of turbulent flows. *Ann. Rev. Fluid Mech.* **16**, 99–137.

SHE, Z.-S., JACKSON, E. & ORSZAG, A. 1990 Intermittent vortex structures in homogeneous isotropic turbulence. *Nature* **344**, 226–228.

SIGGIA, E. D. 1981 Numerical study of small-scale intermittency in three-dimensional. *J. Fluid Mech.* **107**, 375–406.

SIGGIA, E. D. & PATTERSON, G. S. 1978 Intermittency effects in a numerical simulation of stationary three-dimensional turbulence. *J. Fluid Mech.* **86**, 567–592.

SILVEIRA NETO, A., GRAND, D., MÉTAIS, O. & LESIEUR, M. 1991 Large-eddy simulation of the turbulent flow in the downstream region of a backward-facing step. *Phys. Rev. Lett.* **66**, 2320–2323.

SMAGORINSKY, J. S. 1963 General circulation experiments with the primitive equations. I: the basic experiment. *Mon. Weath. Rev.* **91**, 99–163.

SREENIVASAN, K. R. & ANTONIA, R. A. 1977 Skewness of temperature derivatives in turbulent shear flows. *Phys. Fluids* **20**, 1986–1988.

SREENIVASAN, K. R. & TAVOULARIS, S. 1980 On the skewness of the temperature derivative in turbulent flows. *J. Fluid Mech.* **101**, 783–795.

SREENIVASAN, K. R., TAVOULARIS, S., HENRY, R. & CORRSIN, S. 1980 Temperature fluctuations and scales in grid-generated turbulence. *J. Fluid Mech.* **100**, 597–621.

STAQUET, C. & RILEY, J. J. 1989 On the velocity field associated with potential vorticity. *Dyn. Atmos. Oceans* **14**, 93–123.

TAVOULARIS, S., BENNETT, J. C. & CORRSIN, S. 1978 Velocity-derivative skewness in small Reynolds number, nearly isotropic turbulence. *J. Fluid Mech.* **88**, 63–69.

VAN ATTA, C. W. 1971 Influence of fluctuations in local dissipation rates on turbulent scalar characteristics in the inertial subrange. *Phys. Fluids* **14**, 1803–1804; and erratum **16** (1973), 574.

VINCENT, A. & MENEGUZZI, M. 1991 The spatial structure of homogeneous turbulence at Reynolds numbers around 1000. In *Turbulence and Coherent Structures* (ed. O. Métais & M. Lesieur), pp. 191–201. Kluwer.

VOKE, P. R. & COLLINS, M. W. 1983 Large-eddy simulation: retrospect and prospect. *Physico-Chem. Hydrodyn.* **4**, 119–161.

WARHAFT, Z. & LUMLEY, J. L. 1978 An experimental study of the decay of temperature fluctuations in grid-generated turbulence. *J. Fluid Mech.* **88**, 659–684.

WILLIAMS, R. M. & PAULSON, C. A. 1977 Microscale temperature and velocity spectra in the atmospheric boundary layer. *J. Fluid Mech.* **83**, 547–567.

WRAY, A. A. & HUNT, J. C. R. 1990 Algorithms for classification of turbulent structures. In *Topological Fluid Mechanics* (ed. H. K. Moffatt & A. Tsinober), pp. 95–104. Cambridge University Press.

YAKHOT, V. & ORSZAG, S. A. 1986 Renormalization group (RNG) methods for turbulence closure. *J. Sci. Comput.* **1**, 3–52.

YAMAMOTO, K. & HOSOKAWA, I. 1988 A decaying isotropic turbulence pursued by the spectral method. *J. Phys. Soc. Japan* **57**, 1532–1535.

YEH, T. T. & VAN ATTA, C. W. 1973 Spectral transfer of scalar and velocity fields in heated-grid turbulence. *J. Fluid Mech.* **58**, 233–261.